INTERNATIONAL JOURNAL OF HYDROGEN ENERGY 38 (2013) 8664–8682

Available online at www.sciencedirect.com

SciVerse ScienceDirect

journal homepage: www.elsevier.com/locate/he

Redox state-dependent changes in the crystal structure of [NiFeSe] hydrogenase from *Desulfovibrio vulgaris* Hildenborough

*Marta C. Marques, Ricardo Coelho, Inês A.C. Pereira, Pedro M. Matias**

Instituto de Tecnologia Química e Biológica, Universidade Nova de Lisboa, Apartado 127, 2781-901 Oeiras, Portugal

ARTICLE INFO

Article history:
Received 26 November 2012
Received in revised form
10 April 2013
Accepted 22 April 2013
Available online 30 May 2013

Keywords:
Hydrogenase
O_2-tolerance
Catalytic cycle
Structure

ABSTRACT

Hydrogenases are enzymes that can potentially be used in bioelectrical devices or for biological hydrogen production, the most studied of which are the [NiFe] type. Most [NiFe] hydrogenases are inactivated by oxygen and the few known O_2-tolerant enzymes are hydrogen-uptake enzymes, unsuitable for hydrogen production, due to strong product inhibition. In contrast, the [NiFeSe] hydrogenases, where a selenocysteine is bound to the nickel, are very attractive alternatives because of their high hydrogen production activity and fast reactivation after O_2 exposure. Here we report five high-resolution crystallographic 3D structures of the soluble form of the [NiFeSe] hydrogenase from *Desulfovibrio vulgaris* Hildenborough in three different redox states (oxidized as-isolated, H_2-reduced and air re-oxidized), which revealed the structural changes that take place at the active site during enzyme reduction and re-oxidation. The results provide new insights into the pathways of O_2 inactivation in [NiFe], and in particular [NiFeSe], hydrogenases. In addition, they suggest that different enzymes may display different oxidized states upon exposure to O_2, which are probably determined by the protein structure.

1. Introduction

At a critical stage of the fossil fuel crisis and global warming, hydrogen is drawing increased attention as an energy carrier with great potential to become an environment-friendly fuel in the future. However, H_2 production still relies on the thermocatalytic transformation of fossil fuels, because the apparently simple reaction of producing H_2 from H^+ and e^- is in fact very difficult to achieve. Hydrogenases (Hases) are the natural enzymes for the production and oxidation of H_2 in ambient conditions that are far more efficient than Pt-based catalysts, and biological H_2 production offers a promise for H_2 generation using clean technologies and renewable sources [1–3].

Hases are classified according to the metal content of their active site: di-iron ([FeFe]), nickel–iron ([NiFe]), and iron–sulfur cluster free ([Fe]) Hases [4,5]. Among these, the [NiFe] Hases are the most common and most studied enzymes. Based on a phylogenetic and functional analysis, the [NiFe] proteins can be divided into four physiological groups: periplasmic H_2-uptake Hases, cytoplasmic H_2-uptake Hases, cytoplasmic Hases with additional subunits (bidirectional Hases) and energy-converting membrane-bound Hases [4]. The minimum biological unit of [NiFe] Hases is composed of two subunits: the small electron transferring subunit contains three covalently bound iron–sulfur clusters, and the large subunit harbors the bimetallic active site. In the catalytic

Abbreviations: Hase, hydrogenase; Sec, selenocysteine; Tris, tris(hydroxymethyl)aminomethane.

* *Corresponding author*. Tel.: +351 21 4469669; fax: +351 21 4433644.
E-mail address: matias@itqb.unl.pt (P.M. Matias).

0360-3199/$ – see front matter
http://dx.doi.org/10.1016/j.ijhydene.2013.04.132

center, the Ni and Fe atoms are bridged by two cysteines and two other cysteines coordinate the Ni atom.

A major difficulty in the biotechnological application of Hases derives from the fact that O_2 can react with the catalytic center, inactivating the enzymes [6]. Whereas the [FeFe] Hases are irreversibly damaged by O_2, in the [NiFe] enzymes the inactivation is reversible. In H_2-oxidizing aerobic bacteria such as *Ralstonia eutropha*, more O_2 tolerant enzymes are present [2,7–9]. However, these enzymes are designed for H_2 oxidation and exhibit very low H_2 production activities, as well as strong product inhibition by H_2 [10]. The membrane-bound [NiFe] uptake hydrogenases from *Escherichia coli* and *Aquifex aeolicus* also display a high catalytic activity for H_2 oxidation in air [11,12].

The [NiFe] Hases display several redox states. The inactive oxidized states are usually a mixture of Ni-A (unready) and Ni-B (ready) states, both of which are paramagnetic [13]. In the Ni-B state, the enzyme is quickly reactivated upon reduction, whereas the activation of an enzyme in the Ni-A state requires a much longer time period. The crystallographic structures of oxygen-sensitive [NiFe] Hases showed that in the oxidized state an oxygen species is present, bridging the [NiFe] site (reviewed in Ref. [14]). It is currently believed that this ligand is a hydroxide (OH^-) in the Ni-B state [15], whereas the structure of the Ni-A state is still a matter of debate, as a hydroperoxy (OOH^-) ligand was reported for the [NiFe] enzymes from *Desulfovibrio* spp. (reviewed in Ref. [16]), but in *Allochromatium vinosum* hydrogenase a structure of the Ni-A state revealed the presence of only a mono-oxide bridging ligand [17].

Extensive research has been carried out on increasing the O_2-tolerance of [NiFe] Hases. Studies on O_2-sensitive Hases have focused mainly on restricting O_2 access to the active site by narrowing the hydrophobic gas channels leading to it (see e.g., Refs. [12,15,16]), whereas studies on O_2-tolerant Hases have aimed at elucidating the structural basis of O_2 tolerance (see e.g., Refs. [12,18–22]). The crystal structures of three O_2-tolerant [NiFe] Hases have been recently reported [19,22,23], and the proximal iron–sulfur cluster was identified as the structural element responsible for O_2-tolerance. This cluster is coordinated by six cysteine residues instead of the usual four in O_2-sensitive Hases, and one of the sulfido iron ligands is replaced by a cysteine sulfur atom. This unprecedented [4Fe–3S] cluster is proposed to be capable of undergoing two redox transitions (instead of only one in standard [4Fe–4S] clusters), and thus prevents the enzyme from reaching the Ni-A state upon exposure to O_2 [20].

The [NiFeSe] Hases are a sub-group of the [NiFe] enzymes where a selenocysteine (Sec) residue replaces a cysteine as a terminal Ni ligand (reviewed in Ref. [24]). The [NiFeSe] Hases show some unique properties including a higher H_2-production than H_2-oxidation activity [24–27]. Their oxidized states do not display the characteristic Ni-A or Ni-B inactive states after aerobic isolation, typical of O_2-sensitive [NiFe] Hases, and they become active immediately upon reduction. Although it was shown that the [NiFeSe] enzymes from *Desulfomicrobium baculatum* and *Desulfovibrio vulgaris* Hildenborough react with oxygen to produce an inactive state, both enzymes display a very fast reactivation requiring a low redox potential [26,28], suggesting different oxidized species from those formed in standard [NiFe] Hases. In addition, the *Dm. baculatum* [NiFeSe] Hase exhibits less inhibition by H_2 than standard [NiFe] Hases, and it can sustain H_2 production in the presence of low O_2 levels [26]. Overall, these properties make [NiFeSe] Hases very interesting targets for H_2 production. This was recently demonstrated in a system using the *Dm. baculatum* enzyme for photocatalytic H_2 production under non-strict anaerobic conditions [29]. In another application, we observed good electrocatalytic currents for H_2 production from the *D. vulgaris* enzyme bound to a gold electrode [30]. In contrast to a wealth of studies on the O_2 inactivation of [NiFe] Hases [13,31–33] very few studies have addressed the same topic in [NiFeSe] Hases. However, this is an important matter for future biotechnological applications of these enzymes, since they share some of the attractive properties of the O_2-tolerant enzymes (absence of Ni-A species and fast reactivation) and consequently appear to have some level of protection to O_2 exposure [34], while exhibiting much higher H_2 production activities.

The [NiFeSe] Hase from *D. vulgaris* Hildenborough is an example of an enzyme with a high H_2 production activity [25]. *D. vulgaris* is an anaerobic organism containing several different Hases of the [FeFe] and [NiFe] types, and it can use H_2 as an energy source, or grow fermentatively with H_2 production. The [NiFeSe] Hase is the major Hase expressed in *D. vulgaris* when Se is available [35], reflecting its more efficient properties. This enzyme contains a lipidic group bound to the N-terminus of the large subunit that attaches it to the cellular membrane [36]. A soluble form without the lipidic group was also purified, which displayed lower activity [35]. Recently, we determined the crystal structure of the as-isolated oxidized soluble form of the [NiFeSe] Hase [37]. This was the first structure of an oxidized [NiFe] Hase that does not contain an oxide bridging ligand at the active site, confirming it does not form the Ni-A or Ni-B inactive states typical of oxygen-sensitive [NiFe] Hases. An exogenous sulfur atom is present instead, bound to Ni and Se, and causing a side-chain conformation change in the Sec that effectively blocks O_2 access to Ni. However, evidence for O_2 damage to the enzyme was revealed by the fact that the terminal Cys ligand of the Ni was found oxidized to a sulfinate state and the proximal [4Fe–4S] cluster was partially oxidized to [4Fe–3S–3O].

In this work we present five high-resolution crystallographic 3D structures of the soluble form of the *D. vulgaris* [NiFeSe] Hase in several redox states (oxidized as-isolated, H_2-reduced and air re-oxidized), revealing the structural changes that take place at the active during enzyme reduction and re-oxidation. Our results demonstrate the involvement of the proximal [4Fe–4S] cluster in enzyme inactivation after O_2 attack, and the much higher resolution of the oxidized state form obtained in the present work allowed the unambiguous assignment of the structure and stereochemistry of the modified cluster as a [4Fe–4S–3O] center. This oxidative modification is reversed upon reduction, whereas the terminal cysteine linked to the Ni atom is irreversibly oxidized to sulfinate by O_2 attack during the purification and/or crystallization stages of the enzyme. These structural modifications differ from the oxidized states of the [NiFe] hydrogenases described to date, bring new insights into this [NiFe] hydrogenase superfamily, and are fundamental to understand their

properties and for the correct design of devices using these enzymes for H_2 production, particularly in the case of the [NiFeSe] enzymes.

2. Materials and methods

2.1. Protein production, purification and enzymatic activity assay

The soluble form of *D. vulgaris* [NiFeSe] Hase, lacking the first 11 residues of the large subunit and the lipidic group, was isolated and purified as previously described by the authors of Ref. [38].

H_2 production activity was determined by gas chromatography at pH 7.6, as described in Ref. [25], with dithionite as electron donor and in the presence of methyl viologen. The soluble form of *D. vulgaris* [NiFeSe] Hase was diluted 500× in 20 mM Tris buffer pH 7.6 and incubated at 37 °C for 45 min.

To circumvent the low and non-reproducible yield of soluble *D. vulgaris* [NiFeSe] Hase using the previously described protocol [38], this protein was also produced by incubation of the membrane form with a lipase from *Rhizopus niveus* (Sigma). The assay consisted in mixing 50 μM of the membrane form of *D. vulgaris* [NiFeSe] Hase with 5 μg of lipase, in a 20 mM Tris–HCl pH 8.0 buffer, at 37 °C for 12 h. After that time, a yield of almost 99% soluble [NiFeSe] Hase was obtained. The sample obtained was checked for Hase activity and was further purified on a Pharmacia Resource Q column, equilibrated with 20 mM Tris–HCl pH 7.6 buffer, applying a stepwise gradient of 1 M NaCl. The eluted fraction containing pure soluble *D. vulgaris* [NiFeSe] Hase was washed and concentrated to 11 mg/mL in 20 mM Tris–HCl pH 7.6.

2.2. Crystallization and X-ray diffraction data collection

Crystals of the native soluble form of *D. vulgaris* [NiFeSe] Hase were obtained aerobically at room temperature, as previously described [38]. Crystals of the as-isolated, oxidized form were cryoprotected using a solution containing 20% glycerol, 20.5% PEG 1500 (w/v) and 0.1 mM Tris–HCl pH 7.6, flash-cooled in N_2(l) and transferred to a storage dewar. Reduced crystals were prepared from crystals of the oxidized form. The crystals were first transferred to a new drop containing 7 μL of the cryoprotecting solution, to which were added 1 μL of 10 mM methyl-viologen and 50 mM Tris–HCl pH 7.6 buffer. Then, the drop was kept in an anaerobic environment, 15% H_2 and 85% N_2, until the solution and the crystals became completely blue, an indication of their reduced state. The drop containing the reduced crystals was then transferred to an anaerobic glove box, and some of the reduced crystals were harvested, flash-cooled in N_2(l) and stored. The drop with the remaining crystals was subsequently removed from the anaerobic environment, and equilibrated. The re-oxidized crystals were obtained by air oxidation of reduced crystals for 24 h or 48 h at 20 °C, which were then harvested, flash-cooled in N_2(l) and stored. All solutions used in this procedure were degassed with nitrogen prior to their use, and stored under anaerobic conditions. The crystals of oxidized, reduced and re-oxidized *D. vulgaris* [NiFeSe] Hase were transferred to a dry shipper and sent to the PXIII beamline at the Swiss Light Source (SLS) of the Paul Scherrer Institute in Villigen, Switzerland, for data collection. Diffraction datasets were collected from one oxidized (Ox1), one reduced (Red1) and one re-oxidized for 24 h (ReOx24) single crystals of *D. vulgaris* [NiFeSe] Hase. The diffraction pattern of the crystal of re-oxidized for 48 h was multiple and no useful data could be collected.

Crystals of soluble *D. vulgaris* [NiFeSe] Hase prepared from the membrane form by incubation with a commercial lipase were obtained using the sitting-drop vapor diffusion method. 1 μL of a reservoir solution containing 16% PEG 8000 (w/v) and 0.05 M KH_2PO_4 pH 4.1 was mixed with an equal volume of a solution composed of 11 mg/mL protein in 20 mM Tris–HCl buffer pH 7.6, and equilibrated against a 500 μL reservoir. Crystals appeared within 5 days. One crystal of the oxidized form was cryoprotected using a solution containing 20% glycerol, 16% PEG 8000 (w/v) and 0.05 M KH_2PO_4 pH 4.1, flash-cooled in N_2(l) and transferred to a storage dewar. Reduced crystals were obtained from crystals of the oxidized form by incubation in a drop containing 5 μL 16% PEG 8000, 0.05 M KH_2PO_4 pH 4.1 and 20% glycerol, to which were added 0.4 μL of 10 mM methyl-viologen and 0.05 M KH_2PO_4 pH 4.1 buffer, previously flushed with N_2. Subsequently, the drop was kept for 30 min under an anaerobic environment (15% H_2 and 85% N_2) and sodium dithionite was used as reducing agent. Small amounts were added until the solution and the crystals turned blue, taken as an indication of their reduced state. The reduced crystals were quickly harvested, flash-cooled in N_2(l) and stored. These crystals of oxidized and reduced *D. vulgaris* [NiFeSe] Hase were transferred to a dry shipper and sent to the ID29 beamline at the European Synchrotron Radiation Facility (ESRF) for data collection. Diffraction datasets were collected from one oxidized (Ox2) and one reduced (Red2) single crystals of *D. vulgaris* [NiFeSe] Hase. No crystals of re-oxidized protein could be obtained under these conditions, as they re-dissolved a few hours after reduction and removal from the anaerobic environment.

For all datasets, the wavelength was chosen at (SLS) or near (ESRF) the absorption edge K of the selenium atoms. The diffraction images were processed with XDS [39] and conversion of intensities to structure factor amplitudes was carried out with CTRUNCATE in the CCP4 program suite [40]. The data collection and processing statistics are listed in Table 1.

2.3. Structure determination and refinement

The five crystal structures of *D. vulgaris* [NiFeSe] Hase in each of the three redox forms were determined by the molecular replacement method with PHASER [41] via the CCP4 Graphics User Interface [42]. The coordinates of the protein chains of the large and small subunits of the previously published crystal structure of *D. vulgaris* [NiFeSe] Hase (PDB 2wpn) [38] were used as search models, after removal of all non-protein atoms. Also, the side-chain of the Sec residue was truncated after its C^{β} atom prior to the calculations.

The structures were refined with PHENIX [43]. Each PHENIX refinement stage consisted of three cycles with refinement of positional coordinates, individual isotropic atomic

Table 1 – Data collection and processing statistics.

	Oxidized 1, Ox1	Oxidized 2, Ox2	Reduced, Red1	Reduced, Red2	Re-oxidized, ReOx24
Beamline	SLS PXIII	ESRF ID29	SLS PXIII	ESRF ID29	SLS PXIII
Detector	MAR 225 CCD	PILATUS 6M	MAR 225 CCD	PILATUS 6M	MAR 225 CCD
Wavelength (Å)	0.9796	0.9762	0.9796	0.9762	0.9796
Data Processing	XDS/CCP4	XDS/CCP4	XDS/CCP4	XDS/CCP4	XDS/CCP4
Space Group	$P2_12_12_1$	C2	$P2_12_12_1$	$P3_121$	$P2_12_12_1$
Unit cell parameters (Å,°)					
a	72.17	106.69	72.30	61.80	72.27
b	97.35	63.35	96.99	61.80	97.63
c	102.97	109.74	103.86	339.30	103.35
α	90	90	90	90	90
β	90	105.42	90	90	90
γ	90	90	90	120	90
Resolution (Å)[a]	45.5–1.50 (1.54–1.50)	53.9–1.33 (1.41–1.33)	45.8–1.95 (2.07–1.95)	56.6–1.82 (1.93–1.82) [b]	44.1–1.80 (1.91–1.80)
Nr. observations	830460 (41625)	487017 (77560)	194894 (29857)	275858 (33355)	250342 (39571)
Unique reflections	114933 (7556)	159127 (25456)	53472 (8247)	67904 (9884)	64222 (10480)
Multiplicity	7.2 (5.5)	3.1 (3.0)	3.6 (3.6)	4.1 (3.4)	3.9 (3.8)
Completeness (%)	98.6 (88.5)	98.3 (97.5)	99.0 (95.8)	97.7 (89.9)	94.0 (96.3)
R-merge (%) [c]	9.0 (58.9)	3.5 (50.5)	12.8 (49.2)	3.7 (7.9)	6.6 (34.0)
$<I/\sigma(I)>$	17.5 (3.0)	14.2 (1.7)	11.1 (3.3)	23.3 (9.3)	16.2 (4.1)
R-meas (%) [d]	9.8 (65.1)	4.2 (61.3)	15.0 (57.7)	4.2 (9.2)	7.6 (39.2)
Wilson B ($Å^2$)	9.9	15.3	13.9	15.6	14.1
Z[e]	1	1	1	1	1
Estimated V_M[f]	2.18	2.12	2.16	2.22	2.20
Estimated solvent content (%)[f]	43.6	42.0	43.0	44.5	44.0
PDB accession code	3ze6	3ze9	3z37	3zea	3ze8

a Values in parentheses refer to the highest resolution shell.
b The high resolution limit was restricted due to spatial overlaps caused by the long cell axis in an unfavorable orientation.
c R-merge = merging R-factor, $(\Sigma_{hkl}\Sigma_i|I_i(hkl) - <I(hkl)>|)/(\Sigma_{hkl}\Sigma_i I(hkl)) \times 100\%$
d R-meas = redundancy independent R-factor, $\Sigma_{hkl}\,[N/(N-1)]^{1/2}\Sigma_i|I_i(hkl) - <I(hkl)>|/(\Sigma_{hkl}\Sigma_i I_i(hkl)) \times 100\%$ [70]. For each unique Bragg reflection with indices (*hkl*), I_i is the *i*-th observation of its intensity and *N* its multiplicity.
e Nr. molecules in the asymmetric unit.
f According to Matthews coefficient [71].

displacement parameters for all non-hydrogen atoms and also refinement of the anomalous dispersion parameters for the Se atom, followed by model inspection and editing with Coot [44] against sigmaA-weighted $2|F_o| - |F_c|$ and $|F_o| - |F_c|$ electron density maps. Water molecules were added with PHENIX and checked with Coot. In the Ox1, Ox2 and Red2 structures, hydrogen atoms in calculated positions were added to the structural model and included in the refinement. In the Ox2, Red1, Red2 and ReOx24 structures, TLS (translation-libration-screw) rigid body refinement of atomic displacement parameters was carried out, followed by refinement of individual isotropic B-factors. For each crystal structure, the TLS groups were parameterized using the TLS Motion Determination (TLSMD) server [45]. In the Ox1 and ReOx24 structures, 5 incomplete chains of 3-[dodecyl(dimethyl)ammonio]propane-1-sulfonate detergent (SBC), used in the protein purification, were identified in the electron density maps and included in the refinement. The quality of the five refined crystal structures was assessed with MolProbity [46] as included in PHENIX, and the corresponding refinement and validation statistics are presented in Table 2. Occupation factors were refined for three Sec489 conformers in the Ox1 and Ox2 structures, two Sec489 conformers in the Red2 and ReOx24 structures, and two forms of the proximal [Fe–S] cluster in the Ox1 structure. The final occupation factors are listed in Table 3. Figs. 2–9 were generated using PyMOL Molecular Graphics System, Version 1.4.1 (Schrödinger, LLC).

2.4. *Sequence analysis tools*

Sequence data were recovered from the U.S. Department of Energy Joint Genome Institute website (http://www.jgi.doe.gov) and Integrated Microbial Genomes website (http://img.jgi.doe.gov). Multiple alignments were performed using ClustalX [47] and edited with GeneDoc (http://www.psc.edu/biomed/genedoc).

3. Results and discussion

3.1. *Purification and enzymatic activity*

We have never been able to obtain crystals from the native, membrane form of the *D. vulgaris* [NiFeSe] Hase, which contains a lipidic group at the N-terminus of the large subunit [36].

Table 2 – Refinement statistics.

Dataset	Oxidized 1, Ox1	Oxidized 2, Ox2	Reduced, Red1	Reduced, Red2	Reoxidized, ReOx24
Resolution limits (Å)[a]	45.5–1.50 (1.52–1.50)	52.9–1.33 (1.35–1.33)	45.8–1.95 (1.97–1.95)	56.6–1.82 (1.84–1.82)	44.1–1.80 (1.82–1.80)
R_{work}[b]	0.135 (0.240)	0.131 (0.302)	0.153 (0.236)	0.124 (0.146)	0.135 (0.200)
No. reflections in working set[c]	210,208 (5740)	286,382 (8780)	96,625 (2649)	106,181 (2544)	111,795 (3668)
R_{free}[d]	0.154 (0.231)	0.148 (0.307)	0.190 (0.247)	0.147 (0.166)	0.166 (0.244)
Nr. reflections in test set[c]	11,120 (300)	15,046 (451)	5092 (143)	5689 (131)	5953 (182)
Cruickshank DPI (Å)[e]	0.04	0.03	0.10	0.07	0.08
ML coordinate error estimate[f]	0.13	0.11	0.19	0.16	0.14
Model composition and completeness					
Regions omitted	1A–6A, 1B-14B	1A–4A, 1B-14B	1A–6A, 1B–14B	1A–4A, 1B-14B	1A–6A, 1B–14B
Disordered residues	35	34	7	15	16
Non-hydrogen protein atoms[g]	5993	6024	5857	5902	5901
Ligand/ion	40	38	34	35	35
Solvent molecules	700	741	734	637	639
Glycerol	12	–	–	–	-
Detergent	53	–	–	–	49
Mean B values (Å^2)[h]					
Protein main-chain	10.9	19.2	12.5	16.3	13.6
Protein side-chain	14.1	22.3	15.2	20.1	16.7
Ligand/ion	9.2	15.3	11.9	14.3	14.6
Solvent	23.4	33.8	25.7	30.0	26.4
Glycerol	22.3	–	–	–	–
Detergent	31.0	–	–	–	33.3
Model r.m.s. deviations from ideality					
Bond lengths (Å)	0.012	0.012	0.009	0.010	0.009
Bond angles (°)	1.476	1.303	1.148	1.251	1.126
Chiral centers (Å^3)	0.091	0.085	0.075	0.075	0.076
Planar groups (Å)	0.008	0.008	0.006	0.007	0.005
Model validation[i]					
% Ramachandran outliers	0.4	0.4	0.1	0.4	0.1
% Ramachandran favored	97.3	98.0	97.3	97.8	97.3
% Rotamer outliers	1.1	1.2	1.3	1.1	0.8
C^{β} outliers	3	0	0	0	0
Clash score	6.4	4.9	5.3	4.4	5.4
PDB accession ID	3ze6	3ze9	3z37	3zea	3ze8

a Values in parentheses refer to the highest resolution shell.
b $R_{work} = (\Sigma_{hkl}||F_{obs}(hkl)| - |F_{calc}(hkl)||)/(\Sigma_{hkl}|F_{obs}(hkl)|) \times 100\%$.
c The Bijvoet pairs were treated as separate reflections due to the refinement of the anomalous dispersion coefficients for the Se atom.
d R_{free} is calculated as above from a random sample containing 5% of the total number of independent reflections measured.
e DPI is the diffraction-component precision index of the refined atomic coordinates and is estimated from R_{free} by the formula $DPI = (N_i/n_{obs})^{1/2} \times C^{-1/3} \times R_{free} \times d_{min}$ [72], where N_i is the number of non-hydrogen atoms, n_{obs} is the number of reflections included in the refinement, C is the fraction completeness of those reflections and d_{min} the high-resolution limit of the diffraction data.
f Maximum-likelihood estimate by PHENIX.
g Including atoms in the alternate conformations of disordered residues.
h Calculated from isotropic or equivalent isotropic B-values.
i Calculated with MolProbity [46].

For this reason we used the soluble form for crystallographic studies, which does not have the lipidic group or the first 11 residues of the catalytic subunit. The soluble form exhibits a lower activity than the membrane form, supporting the notion that the lipidic group and/or the first 11 N-terminal residues are somehow important for retaining a high catalytic activity. The native soluble *D. vulgaris* [NiFeSe] Hase used for crystallization displayed a specific activity of 860 U mg^{-1} for H_2 production, quantified by gas chromatography, whereas the H_2 production activity of the membrane form has been reported to be 6910 U mg^{-1}, under the best conditions [25]. To obtain more of the soluble protein we developed an in vitro enzymatic assay to promote cleavage of the N-terminal peptide, in which the membrane form was digested with a commercial lipase from *R. niveus* (Sigma–Aldrich). Complete conversion of the membrane $[NiFeSe]_m$ Hase to active, soluble $[NiFeSe]_s$ Hase form (Fig. 1) was obtained after a 12 h incubation at 37 °C. This procedure allowed the *in vitro* production of

Table 3 – The active site and the proximal [Fe–S] cluster in the different redox states of the of *D. vulgaris* [NiFeSe] Hase.

NiFeSe active site	Oxidized state		Reduced state		Reoxidized state
	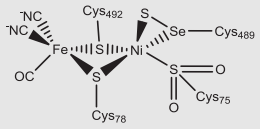		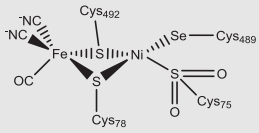		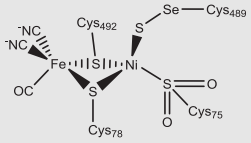
	Conformer I		Conformer III		Conformer II
Structure	Ox1	Ox2	Red1	Red2	ReOx24
% Conformer I	74	73	–	–	–
% Conformer II	16	13	–	12	38
% Conformer III	10	14	100	88	62
Proximal [4Fe–4S]	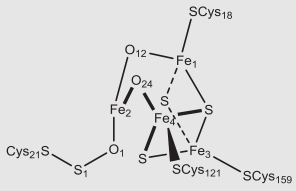		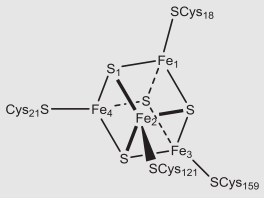		
	[4Fe–4S–3O]		[4Fe–4S]		
	Oxidized state		Reduced state		Reoxidized state
Structure	Ox1	Ox2	Red1	Red2	ReOx24
% [4Fe–4S–3O]	80	100	–	–	–
% [4Fe–4S]	20	–	100	100	100

higher quantities of active soluble *D. vulgaris* [NiFeSe] Hase from its membrane form which, after chromatographic purification, was also used for crystallization. The use of a lipase in an enzymatic assay such as described here has great potential application for the conversion of other lipoproteins into their respective soluble forms.

3.2. *Structure of* D. vulgaris *[NiFeSe] Hase*

As previously reported [37], the overall 3D structure of the *D. vulgaris* [NiFeSe] Hase (Fig. 2) is identical to that of a typical [NiFe] Hase: it is formed by two subunits, of which the larger contains the binuclear [NiFe] catalytic site, and the smaller contains three [Fe–S] clusters. Five crystal structures of the soluble *D. vulgaris* [NiFeSe] Hase in three redox forms were obtained. Three of these resulted from the crystallization of soluble enzyme isolated directly from cell extracts: the as-isolated oxidized (Ox1), reduced (Red1) and re-oxidized (ReOx24) forms. Additionally, two more datasets were collected from crystals of soluble *D. vulgaris* [NiFeSe] Hase prepared from the membrane form by incubation with lipase: one oxidized (Ox2) and one reduced (Red2). All five crystal structures contain a single *D. vulgaris* [NiFeSe] Hase heterodimer in their asymmetric unit. The small and large subunits were designated chains A and B, respectively, and in the remainder of this text these chain identifiers are appended to the residue numbers to indicate which subunit they belong to.

All crystal structures reported herein were compared by superposition using the secondary structure matching algorithm [48] as implemented in the CCP4 suite. The as-isolated oxidized Ox1 structure was used as reference and each chain (A or B) was individually superposed. The results (Supplementary Table 1) show that the largest differences occur between the small chains of the as-isolated oxidized Ox2, reduced Red1 and Red2 crystal structures and the corresponding chains in the as-isolated oxidized Ox1 and re-oxidized ReOx24 crystal structures. The differences are most pronounced in the N-terminal region of the small subunit that is visible in the electron-density maps (residues 7A–9A in Ox1, Red1 and ReOx24, 5A–9A in Ox2 and Red2) and in residues 29A–42A, which form a α-helix near the N-terminus. These differences are caused by the presence in the Ox1 and ReOx24 structures of four Sulfobetaine 3–12 detergent molecules, in two hydrophobic pockets. This detergent, also known as Zwittergent 3–12, was used in the purification of the *D. vulgaris* membranes, from which the soluble form (leading to crystals of Ox1, Red1 and ReOx24) was isolated [25,38]. These chains are not present in the Ox2, Red1 and Red2 structures. The lipase digestion of the membrane protein and subsequent purification (leading to crystals that gave the Ox2 and Red2 structures) removed all traces of detergent from the sample, as expected. However, since the crystals leading to the Ox1, Red1 and ReOx24 structures were obtained from the same protein batch of protein purified from cell membranes, it is not clear why there are no detergent molecules in the Red1 crystal

Fig. 1 – Activity-stained native PAGE. 1. *D. vulgaris* [NiFeSe]$_m$ Hase; 2. *D. vulgaris* [NiFeSe]s Hase; 3. 50 μM of membrane *D. vulgaris* [NiFeSe] Hase incubated with 5 μg of lipase from *Rhizopus niveus* (10 mg/mL), at 37 °C, during 12 h in 20 mM Tris–HCl pH 7.6 buffer.

structure. The larger hydrophobic pocket in the Ox1 and ReOx24 structures contains three sulfobetaine 3–12 molecules and is located at the interface between the two subunits, but only residues 29A–42A were affected. The smaller pocket contains only one sulfobetaine 3–12 molecule, which influenced the conformation of the N-terminus of the small subunit. A fifth sulfobetaine 3–12 molecule is present in a third pocket located in the large subunit of Ox1 and ReOx24, but it does not introduce significant structural differences between the crystal structures.

3.3. *The structure of the active site in the different redox forms*

The NiFe active site is anchored to the protein chain of the large subunit by two cysteine residues, 78B and 492B, which form thiolate bridges between the two metals, whereas the Ni atom is further ligated by Cys75B and Sec489B, and the Fe atom has the characteristic one CO and two CN^- diatomic ligands (Fig. 2).

The Selenocysteine ligand to the Ni, Sec489B, is found to be present in three distinct conformers in the oxidized state, as previously reported [37], where in two of them the Se atom is bound to an exogenous sulfur atom (Table 3 and Fig. 3). In both Sec489B conformers I and II the position of the S atoms is nearly the same, and the Se atom effectively shields the Ni atom in the active site from access by small diatomic molecules such as O_2 [37]. In conformer I both Se and S atoms coordinate Ni, while in conformer II only the S atom is bonded to Ni, and in conformer III no S atom is present and only Se binds Ni. Conformer III of Sec489 is the same as found for the equivalent Cys residue in the oxidized and reduced forms of [NiFe] Hases. In both structures of the as-isolated oxidized

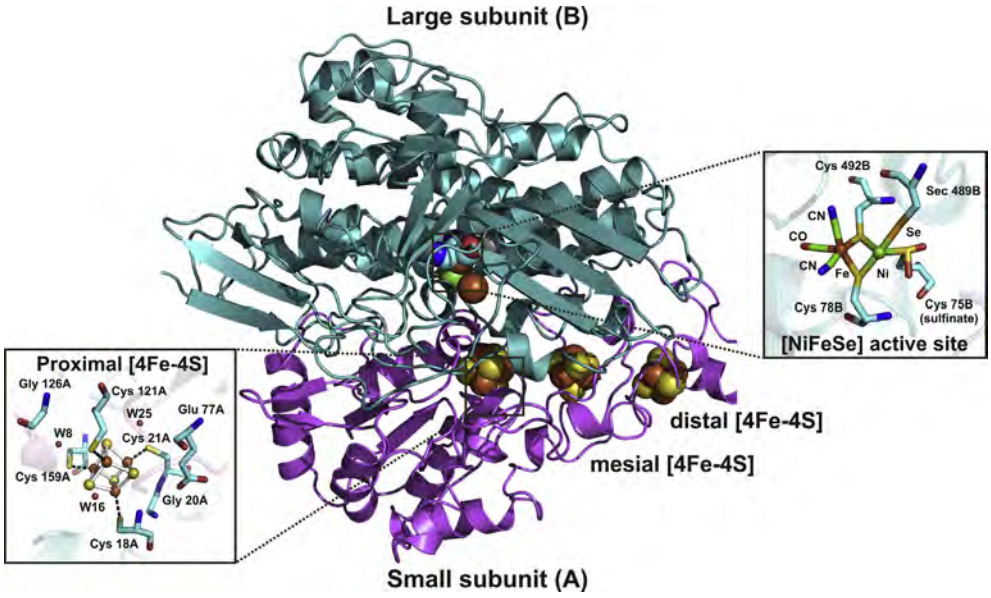

Fig. 2 – The overall structure of the [NiFeSe] Hase from *D. vulgaris* Hildenborough in the reduced state. The boxes show close-up views of the [NiFeSe] active site and the proximal [4Fe–4S] cluster, where the protein residues are drawn in stick representation, and the nickel, iron atoms and conserved water molecules are drawn as spheres. The proximal [4Fe–4S] cluster is drawn in ball-and-stick representation. Atom colors are cyan for carbon, blue for nitrogen, red for oxygen, yellow for sulfur, orange for iron, green for nickel and gold for selenium. The additional H_2S molecule is represented in gray. (For interpretation of the references to color in this figure legend, the reader is referred to the web version of this article.)

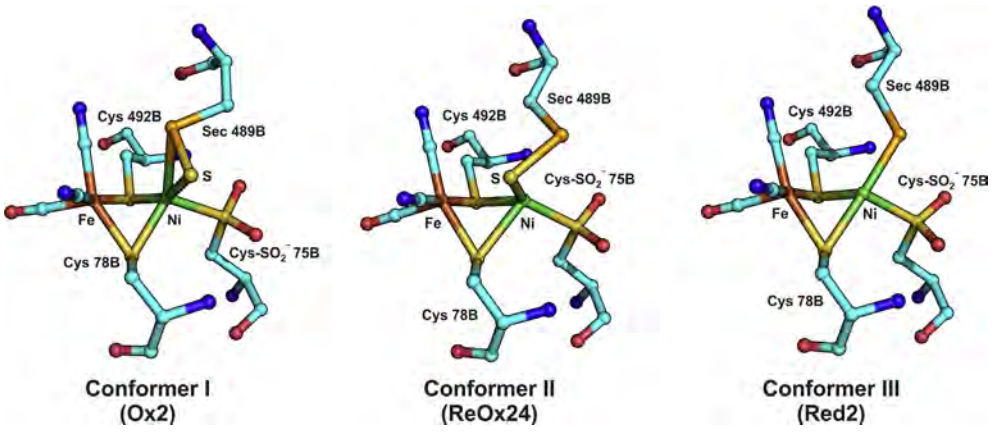

Fig. 3 – Overview of the active site structure of the active site in the different redox states of *D. vulgaris* [NiFeSe] Hase. The [NiFe] center and the protein residues are drawn in ball-and-stick representation, with atom colors cyan for carbon, blue for nitrogen, red for oxygen, yellow for sulfur, orange for iron, green for nickel, gold for selenium. (For interpretation of the references to color in this figure legend, the reader is referred to the web version of this article.)

forms Ox1 and Ox2, the three conformers of Sec489B are present, but with a predomination of conformer I (Fig. 4).

In the reduced Red1 structure the exogenous sulfur atom is no longer observed at the active site and the Sec489B residue is present in conformer III, in agreement with our earlier proposal that conformer III corresponds to the reduced state of the enzyme [37], by analogy with the crystal structure of the reduced *Dm. baculatum* enzyme [49]. In the Red1 structure the active site is present in this single conformation, whereas in the reduced Red2 structure (Fig. 5), a small positive residual electron density region near conformer III of Sec489B was attributed to a slight contribution from conformer II (*ca.* 12%), included in the final PHENIX refinement, which may have been due to some partial re-oxidation during manipulation of the crystal.

Finally, in the re-oxidized structure ReOx24 (Fig. 6) a higher percentage of molecules (38%) include the exogenous sulfur atom at the active site (conformer II), but conformer III is surprisingly still predominant (62% occupancy). No conformer I is present, which agrees with the FTIR results showing that the re-oxidized protein is in a different form from the as-isolated one [28]. After a 24 h exposure to air the enzyme active site will most certainly be fully oxidized, therefore the observed predominance of conformer III suggests that the different conformers do not correlate directly with the oxidation state of the active site, but are rather related to the binding of the exogenous S atom. These observations can be rationalized by considering that reduction leads to displacement of this atom from the active site. Upon re-oxidation, the re-binding of this S atom is a slow process, justifying why 62% of the molecules in the re-oxidized state and ~10% in the oxidized as-isolated state are still found as conformer III, with no bound S. The conformer interconversion indicates that the S atom must remain bound to the protein and very likely occupies a position *ca.* 7.3 Å away from the Ni atom, in a solvent-accessible pocket, which in the Ox1, Ox2 and ReOx24 crystal structures is occupied by a Cl^- ion from the crystallization buffer. Although a proper anion transfer channel could not be identified in the crystal structures, the proposed coordination position for the sulfide ligand is located sufficiently close to the active site, such that protein dynamics due to thermal motion at room temperature should allow the displacement of the sulfide ligand between the active site and this other position. As previously noted [37] the three Sec489 conformers with similar relative occupancies were also observed in a crystal structure of the as-isolated oxidized form of *D. vulgaris* [NiFeSe] Hase obtained from 2.4 Å diffraction data measured *in house*. This rules out the possibility that the observation of conformer III in the Ox1 and Ox2 crystal structures is an artifact caused by photoelectron reduction in the intense synchrotron X-ray beam.

The anomalous dispersion properties of the Se atom in Sec489B were enhanced by the X-ray wavelengths used in the data collections and required a modified refinement procedure. These properties were also helpful to confirm that the residual peaks observed around the main Sec489B conformation in the Ox1, Ox2 (Fig. 4B), Red2 (Fig. 5B) and ReOx24 (Fig. 6B) crystal structures were indeed alternative positions for the Se atom, thus validating the presence of the other conformers (see Supplementary Results for details).

To our knowledge, the unusual double coordination of the Ni atom by a S and Se atoms has not been reported for any other protein structure, and a Cambridge Structural Database [50,51] search for similar coordination motifs in small molecule compounds failed to give any results. However, there were several examples of double coordination of S–Se ligands to transition metal molybdenum, but only if the carbon atom bonded to Se was excluded from the search fragment (see Supplementary Results for details).

In the active site, several bond distances were refined using soft restraints, using large e.s.d. values (0.15 Å), to allow for a wider variation of the restrained bonds and ensuring a well-behaved refinement while avoiding the imposition of a fixed stereochemistry (see Supplementary Results). The mean Ni–Fe distance from the two oxidized structures is 2.42 Å and that from the two reduced structures is 2.50 Å, in agreement with the 2.53 Å observed in the reduced crystal structure of *Dm. baculatum* [NiFeSe] Hase [49]. Surprisingly, in the re-oxidized crystal structure, the Ni–Fe distance increased

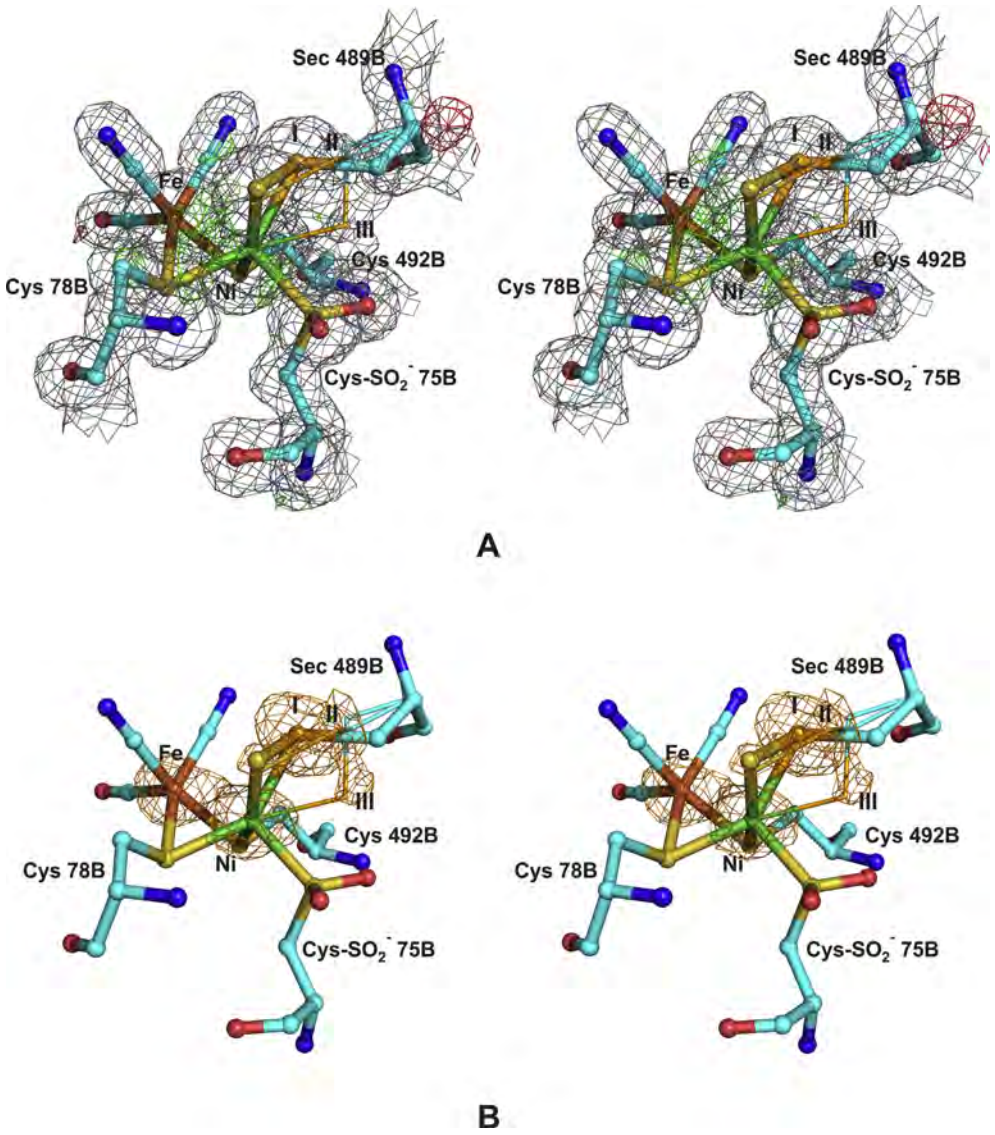

Fig. 4 – Stereoviews of the active site in the oxidized Ox2 structure of *D. vulgaris* [NiFeSe] Hase. The [NiFe] center and the protein residues are drawn in ball-and-stick representation, with atom colors cyan for carbon, blue for nitrogen, red for oxygen, yellow for sulfur, orange for iron, green for nickel, gold for selenium. The roman numerals denote the Se atom position in each of the three Sec conformers in this crystal structure and the two minor Sec conformers are shown as thin lines. (A) The final $2|F_o| - |F_c|$ map is drawn in gray at the 1.5 map r.m.s. level and the final $|F_o| - |F_c|$ map is represented at the 3 (green) and −3 (red) map r.m.s. level. (B) The final anomalous difference map is shown in orange at the 4.5 map r.m.s. level. (For interpretation of the references to color in this figure legend, the reader is referred to the web version of this article.)

further to 2.68 Å. Higher-resolution crystal structures of the reduced and reoxidized forms of *D. vulgaris* [NiFeSe] Hase are needed to validate the significance of the observed variations, but they suggest a behavior of the Ni–Fe core in the active site that is different from that in O_2-sensitive and O_2-tolerant [NiFe] Hases: in these enzymes, the Ni–Fe distance decreases from 2.8–2.9 Å to *ca.* 2.5–2.6 Å when the enzyme loses its bridging ligand by reduction and increases back upon re-oxidation. In contrast, the Ni–Fe distance in *D. vulgaris* [NiFeSe] Hase increases slightly upon reduction and increases even further when the enzyme becomes reoxidized. This different behavior may result from the conformational flexibility displayed by Sec489B (absent in [NiFe] Hases), combined with the chemical nature of the different ligands present in the oxidized state of the enzymes: a bridging oxygen species in O_2-sensitive and O_2-tolerant [NiFe] Hases and an exogenous sulfur atom bound to the Ni atom in *D. vulgaris* [NiFeSe] Hase.

To date it was not possible to obtain crystals after re-oxidation for periods longer than 24 h, in order to investigate whether conformer II eventually converts back into conformer I, the predominant conformer observed in the oxidized, as-isolated form of the *D. vulgaris* [NiFeSe] Hase. Nevertheless, these results agree with the previous FTIR studies which

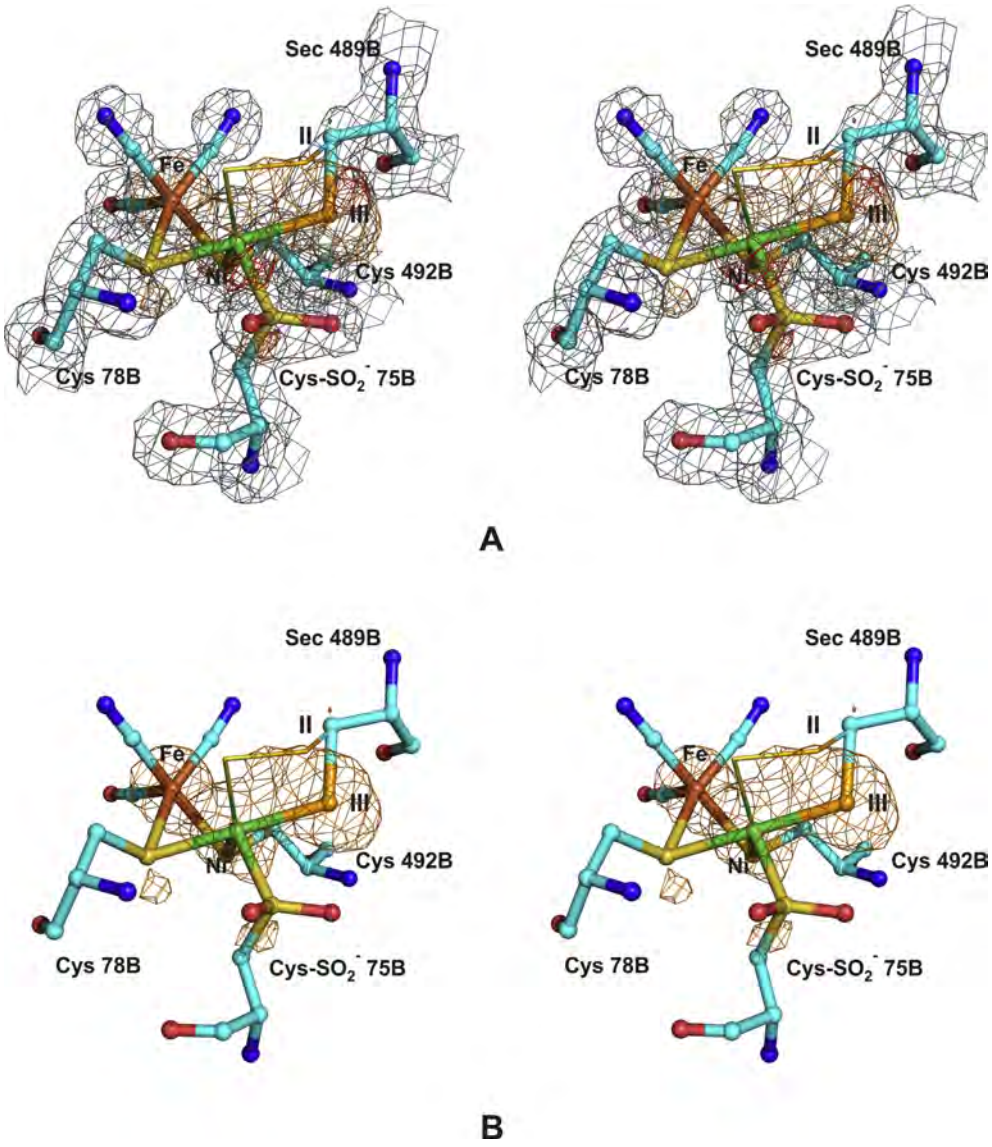

Fig. 5 – Stereoviews of the active site in the reduced Red2 structure of *D. vulgaris* [NiFeSe] Hase. The [NiFe] center and the protein residues are drawn in ball-and-stick representation, with atom colors cyan for carbon, blue for nitrogen, red for oxygen, yellow for sulfur, orange for iron, green for nickel, gold for selenium. The roman numerals denote the Se atom position in each of the two Sec conformers in this crystal structure and the minor Sec conformer present is shown as thin lines. (A) The final $2|F_o| - |F_c|$ map is drawn in gray at the 1.5 map r.m.s. level and the final $|F_o| - |F_c|$ map is represented at the 3 (green) and −3 (red) map r.m.s. level. (B) The final anomalous difference map is shown in orange at the 4.5 map r.m.s. level. (For interpretation of the references to color in this figure legend, the reader is referred to the web version of this article.)

showed that this hydrogenase formed a state different from the as-isolated one upon reduction and re-oxidation [28], and reveal a remarkable structural complexity of the active site of this enzyme upon O_2 inactivation. It was previously shown that in O_2-sensitive [NiFe]-hydrogenases oxidation may generate two different Ni (III) inactive states, Ni-A or Ni-B [32,52]. This is in contrast with [NiFeSe] Hases from *D. vulgaris* and *Dm. baculatum*, which do not form Ni-A or Ni-B species even after reduction and exposure to oxygen [25,49]. In agreement with this, the bridging oxide ligand between the Ni and the Fe is absent in the three redox forms of the *D. vulgaris* enzyme. It seems that the [NiFeSe] Hases form distinct unready states from the O_2-sensitive [NiFe] ones. This is also reflected in the fact that the reactivation of these unready states is fast and requires a low redox potential [26,28].

3.4. *An oxidized cysteine is present in the active site*

We previously reported that Cys75B, one of the terminal cysteines that bind the active site Ni atom, was found oxidized to cysteine sulfinic acid (Cys-SO_2H/Cys-SO_2^-) in the structure of the as-isolated oxidized form of *D. vulgaris* [NiFeSe] Hase [37]. This residue modification is also present in the five crystal structures reported herein. Several crystal structures

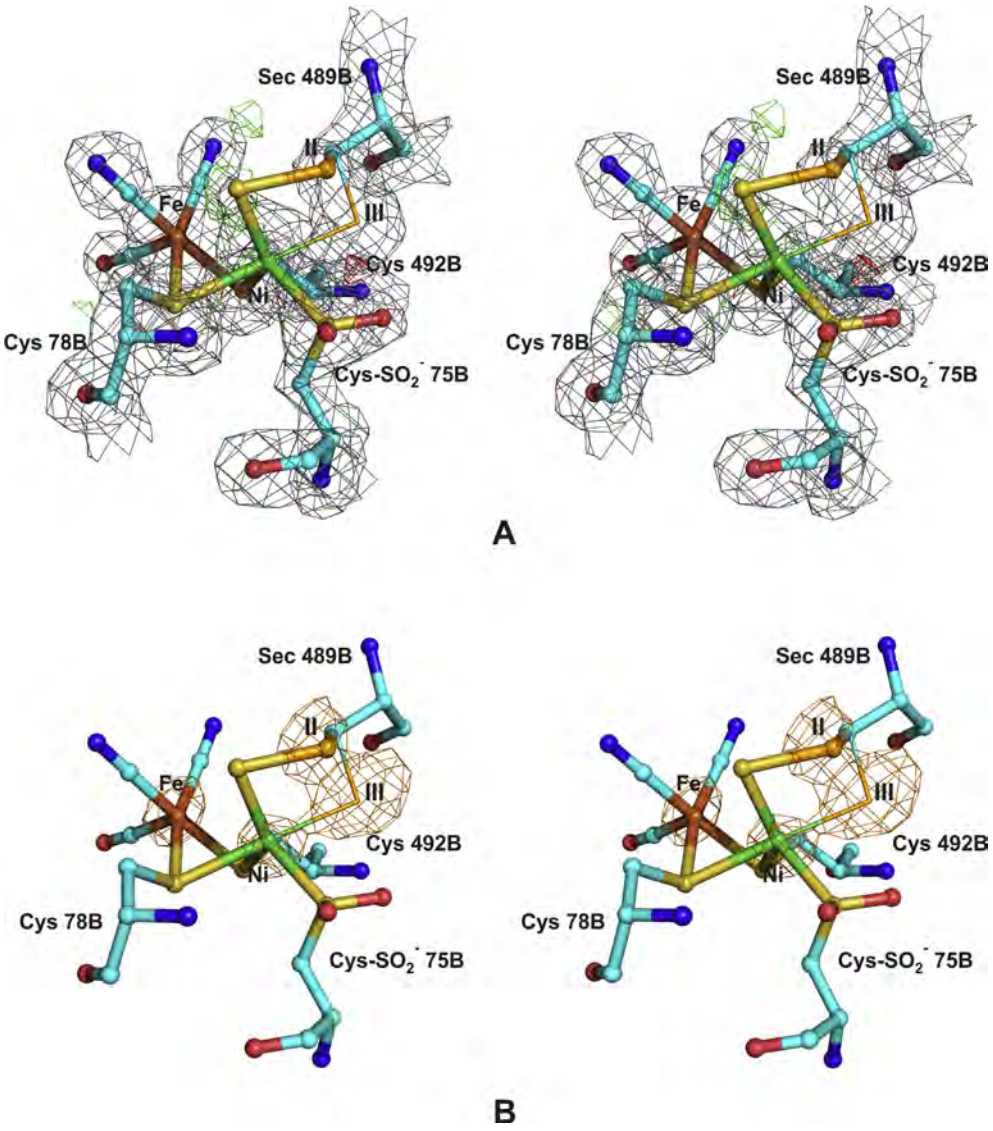

Fig. 6 – Stereoviews of the active site in the re-oxidized ReOx24 structure of *D. vulgaris* [NiFeSe] Hase. The [NiFe] center and the protein residues are drawn in ball-and-stick representation, with atom colors cyan for carbon, blue for nitrogen, red for oxygen, yellow for sulfur, orange for iron, green for nickel, gold for selenium. The roman numerals denote the Se atom position in each of the two Sec conformers in this crystal structure and the still dominant Sec conformer III is shown as thin lines. (A) The final $2|F_o| - |F_c|$ map is drawn in gray at the 1.5 map r.m.s. level and the final $|F_o| - |F_c|$ map is represented at the 3 (green) and −3 (red) map r.m.s. level. (For interpretation of the references to color in this figure legend, the reader is referred to the web version of this article.)

with oxidized cysteines have been described in the literature [53–56]. Oxidation of cysteine thiols to disulfides (–S–S) or sulfenic acids (Cys-SOH) can be carried out by reactive oxygen species (ROS) and reactive nitrogen species (RNS) such as hydrogen peroxide or nitrogen dioxide [57]. This process is reversible, in contrast to oxidation of cysteines to sulfinic ($-SO_2H$) or sulfonic acids ($-SO_3H$), which is regarded as irreversible [57,58]. However, in the case of peroxiredoxins formation of cysteine sulfinic acids was shown to be a reversible process *in vivo* [54]. In the present case, even though all the experiments to reduce the crystals were performed with dithionite and/or in an environment rich in H_2 and N_2, it is evident that the modified cysteine was not reduced, which supports the notion that this modification is irreversible. This process likely occurred during purification and/or crystallization, as cysteines can be selectively oxidized to cysteine sulfinic acid (Cys-SO_2H) and to cysteine sulfonic acid (Cys-SO_3H), even by air [53]. The successful reduction of Ox1 crystals (with a 100% oxidation of Cys75B to sulfinate) with a H_2/N_2 mixture to produce the crystal used in the Red1 structure determination suggests that some enzyme activity was still present in the crystals, since before reduction the crystals were transferred to a fresh drop without free enzyme in solution. It has been suggested that in O_2-sensitive [NiFe] Hases oxidation of a terminal cysteine to sulfenate is related to the formation of the inactive Ni-A state (reviewed in Ref. [59]).

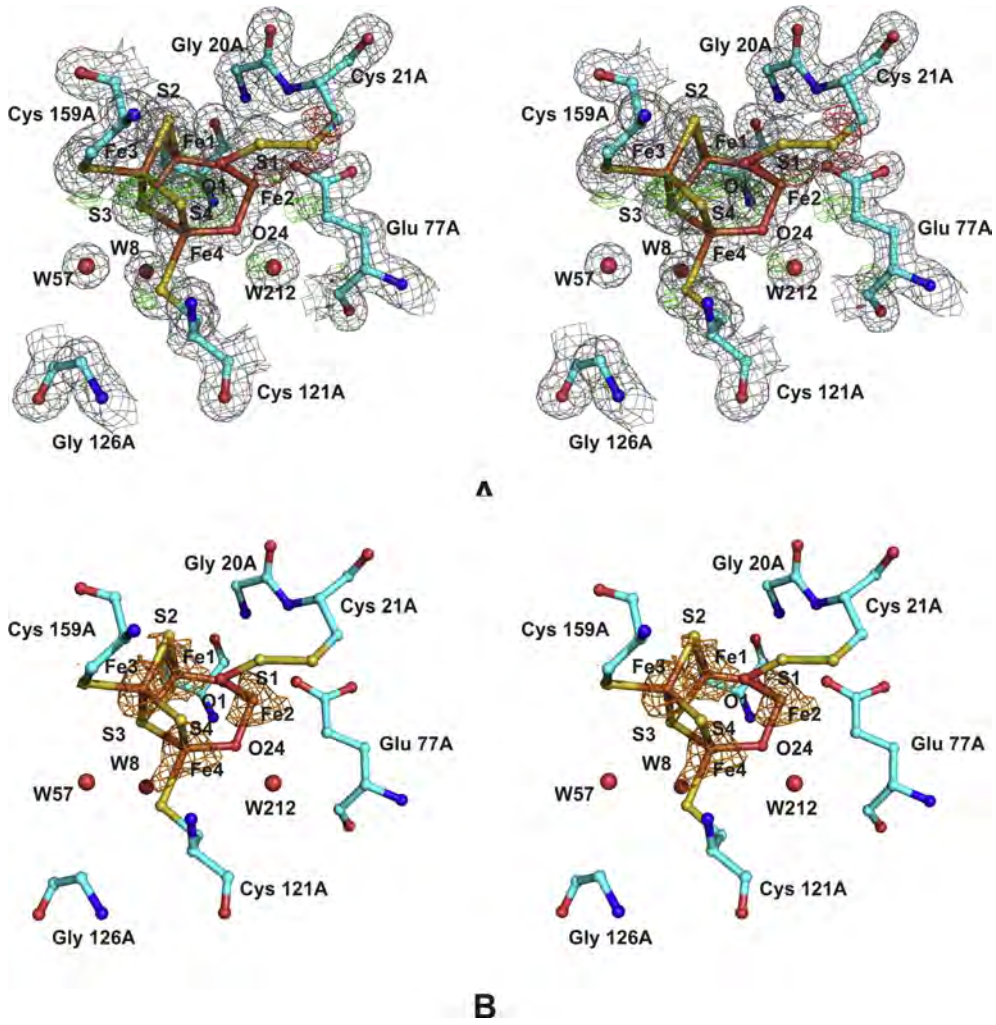

Fig. 7 – Stereoviews of the proximal [Fe4–S4–O3] cluster in the oxidized Ox2 structure of *D. vulgaris* [NiFeSe] Hase. The [Fe–S] cluster and the protein residues are drawn in ball-and-stick representation, and conserved water molecules are drawn as spheres. Atom colors are cyan for carbon, blue for nitrogen, red for oxygen, yellow for sulfur, orange for iron. (A) The final $2|F_o| - |F_c|$ map is drawn in gray at the 1.5 map r.m.s. level and the final $|F_o| - |F_c|$ map is represented at the 3 (green) and −3 (red) map r.m.s. level. (B) The final anomalous difference map is shown in orange at the 4.5 map r.m.s. level. (B) The final anomalous difference map is shown in orange at the 4.5 map r.m.s. level. (For interpretation of the references to color in this figure legend, the reader is referred to the web version of this article.)

However, while the O_2-sensitive [NiFe] Hases in the Ni-A state are inactive, our results suggest that the formation of a cysteine sulfinate in the [NiFeSe] Hase from *D. vulgaris* Hildenborough may not totally abolish enzyme activity. Nevertheless, and although the cysteine sulfinate seems to be present with 100% occupancy in all crystal structures so far determined for this enzyme, the presence of a small number of molecules with non-oxidized cysteines in the crystal cannot be ruled out. These molecules might then reduce the rest by electron transfer in the crystal. Further studies will be required to clarify this point.

In peroxiredoxins the biological relevance of cysteine-sulfinic acids has been well established, and understood as an alteration that results in protection against cellular oxidative stress [60]. In these cysteine-based peroxidases, the cysteine-sulfinic acid residues are exposed near the protein surface and can be reduced back to cysteines via a complex mechanism involving specific enzymes and requiring ATP [60]. In the *D. vulgaris* [NiFeSe] Hase, not only Cys75B is deeply buried inside the protein so that such a reduction process is unlikely, but no evidence exists in the genome of *D. vulgaris* Hildenborough for these cysteine-sulfinic acid-reducing enzymes.

There are no other known protein structures to date displaying a sulfinic acid coordination to Ni as found in the *D. vulgaris* [NiFeSe] Hase crystal structures reported in this work. However, several small molecular compounds with a similar Ni coordination could be found in the Cambridge Structural Database [50,51] (see Supplementary Results for details). The study of these compounds has been stimulated by their role as models for the active site of [NiFe] Hases, and the possibility that oxidation of the thiolate ligands to sulfenates or sulfinates could lead to enzyme inactivation has

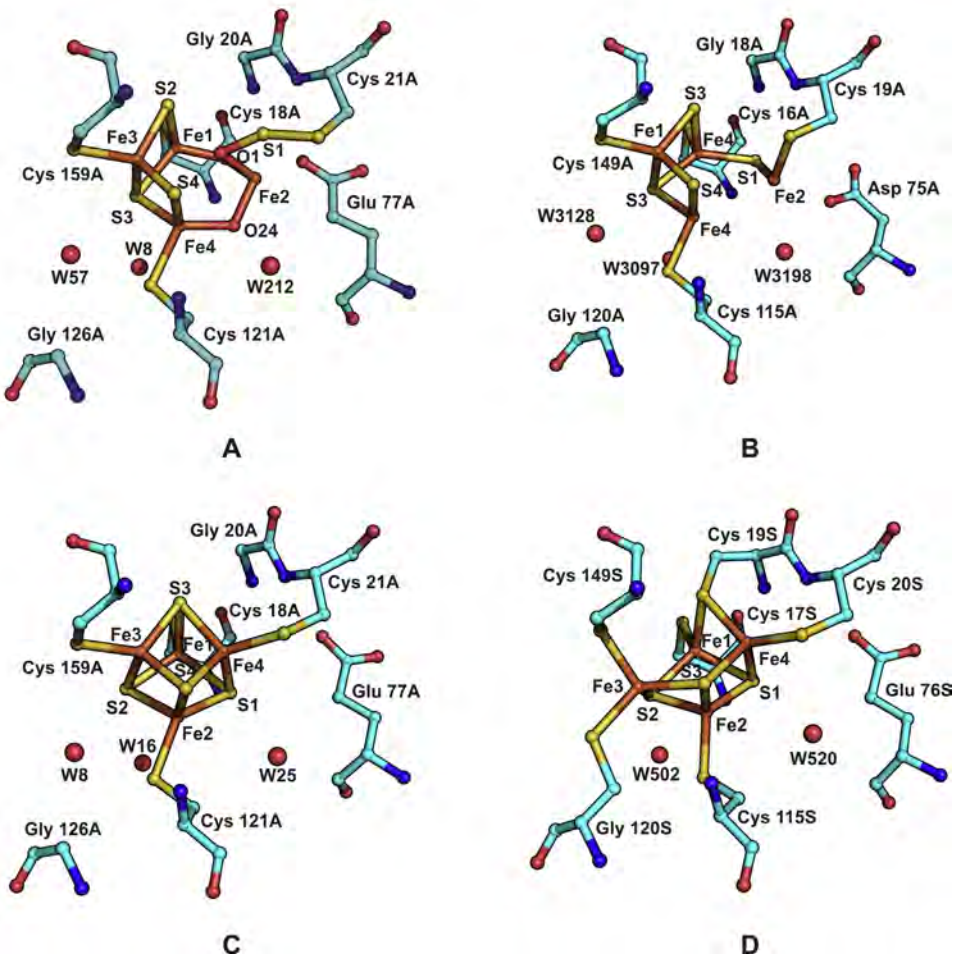

Fig. 8 – Overview of the proximal [Fe–S] cluster in structures of [NiFeSe] Hase from *D. vulgaris* Hildenborough and [NiFe] Hases from *A. vinosum* and *E. coli*. (A) The [Fe4–S4–O3] form in the Ox2 crystal structure; (B) The distorted [Fe4–S4] in the crystal structure of the O_2-sensitive *A. vinosum* [NiFe] Hase in the Ni-A state (PDB 3myr); (C) The cubane [Fe4–S4] form in the Red2 crystal structure; (D) The [4Fe–3S] in the crystal structure of the O_2-tolerant *E. coli* [NiFe] Hase in the reduced state (PDB 3uqy). The [Fe–S] clusters and the protein residues are drawn in ball-and-stick representation, and conserved water molecules are drawn as spheres. Atom colors are cyan for carbon, blue for nitrogen, red for oxygen, yellow for sulfur, orange for iron. (For interpretation of the references to color in this figure legend, the reader is referred to the web version of this article.)

been long recognized (see for example Ref. [61]). Most of these compounds involve a diazo-dithiolate Ni coordination, but there are a few Ni-tetrathiolate molecules [62–64] where one or two sulfinate groups coordinate the Ni atom. Several diazo-dithiolate-Ni complexes with thiolate, sulfenate and sulfinate Ni ligands were studied electrochemically [61] and all show a reversible Ni(II)/Ni(I) redox transition. The oxidation scans of the sulfenate and sulfinate complexes showed irreversible transitions (not present in the scan of the sulfinate complex) that could correspond to the oxidation to sulfinate of the thiolate/sulfenate Ni ligands, and although a further feature was observed at even more positive potentials that might correspond to the Ni(II)/Ni(III) transition, it could not be validated chemically. A tetrathiolate-Ni compound with sulfinate Ni ligands was recently studied electrochemically and the results show only a quasi-reversible Ni(II)/Ni(III) redox transition [64]. Since the experiment only scanned positive potentials, the possibility of a Ni(II)/Ni(I) transition was not investigated. These results raise the possibility that in a [NiFeSe] Hase active site with a cysteine sulfinic acid ligand the Ni atom could still experience the same +1, +2 and +3 redox states as in a pristine active site. However, the transition potentials at which these transitions may occur could be sufficiently changed to cause the enzyme to be inactive.

3.5. *The proximal iron–sulfur cluster*

In O_2-sensitive [NiFe] and in [NiFeSe] Hases, the proximal [4Fe–4S] cluster is cubane-shaped and coordinated by four cysteine residues (Cys 17A, Cys 21A, Cys 115A and Cys 149A in *D. vulgaris*). In the previously reported structures of the oxidized [NiFe] Hase from *D. desulfuricans* ATCC 27774 (1.8 Å)

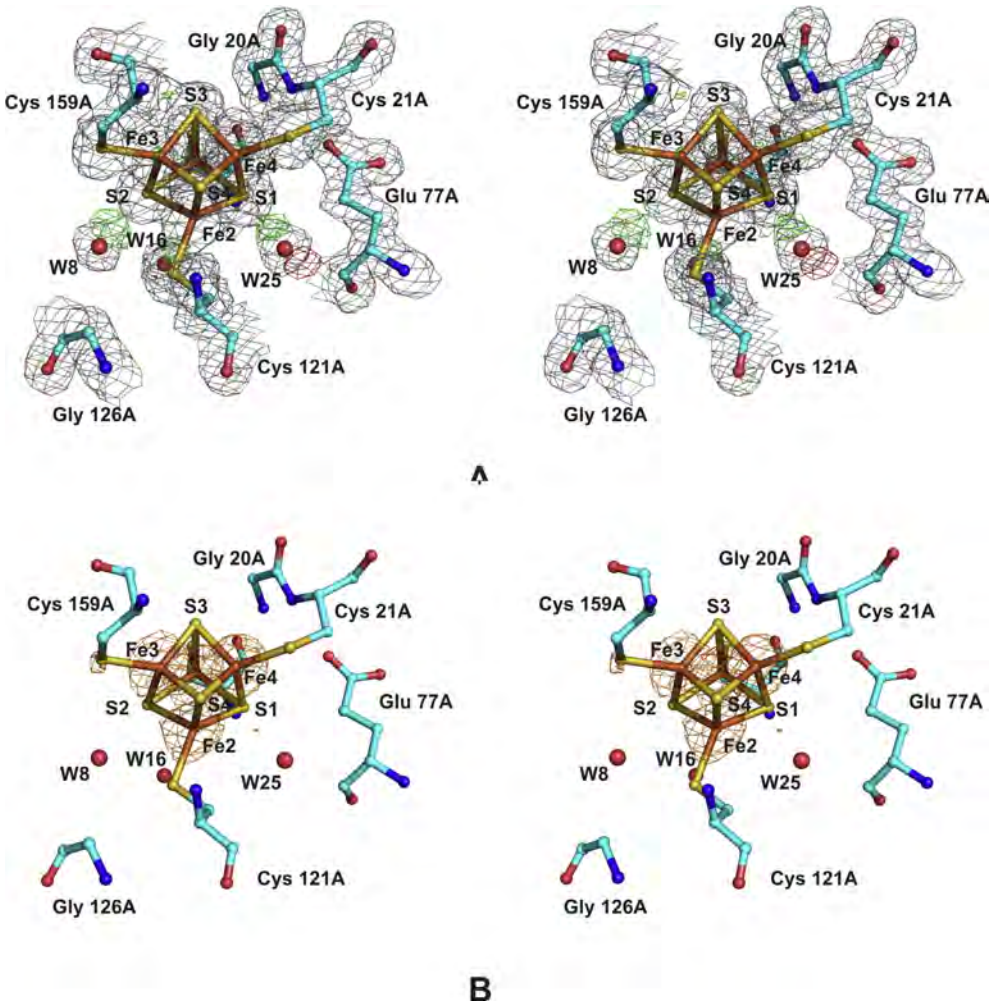

Fig. 9 – Stereoviews of the proximal [Fe4–S4] cluster in the reduced Red2 structure of *D. vulgaris* [NiFeSe] Hase. The [Fe-S] cluster and the protein residues are drawn in ball-and-stick representation, and conserved water molecules are drawn as spheres. Atom colors are cyan for carbon, blue for nitrogen, red for oxygen, yellow for sulfur, orange for iron. (A) The final $2|F_o| - |F_c|$ map is drawn in gray at the 1.5 map r.m.s. level and the final $|F_o| - |F_c|$ map is represented at the 3 (green) and −3 (red) map r.m.s. level. (B) The final anomalous difference map is shown in orange at the 4.5 map r.m.s. level. (For interpretation of the references to color in this figure legend, the reader is referred to the web version of this article.)

[65] and the *D. vulgaris* [NiFeSe] Hase (2.04 Å) [37], the proximal iron–sulfur cluster was found in a partially oxidized form, identified as [4Fe–3S–3O] on the basis of its electron density. A modification of the proximal [4Fe–4S] cluster was also reported for the 3D structure of the membrane-bound O_2-sensitive [NiFe] Hase from *A. vinosum* in the oxidized Ni-A state [17]. However, the partial occupancy of the modified form combined with the 2.1 Å resolution of this structure did not allow a clear identification of the stereochemistry of the modified cluster. A similar oxidative modification has also been reported for a different type of Fe–S cluster in the crystal structure of the oxidized form of the Hybrid Cluster Protein from *D. vulgaris* Hildenborough [66].

In *D. vulgaris* Hildenborough [NiFeSe] Hase, the high resolution (1.5 Å) electron density maps of the as-isolated Ox1 crystal structure allowed for the first time a complete and detailed picture, revealing that in this case the cluster is super-oxidized to [4Fe–4S–3O] (Fig. 7). Three of its iron atoms are bound to cysteine residues (Cys 17A, Cys 115A and Cys 149A) and the fourth is coordinated by three oxygen atoms and one of the carboxylate oxygens of Glu 77A (Fig. 8A). This iron atom occupies a very similar position to that of Fe2 in the modified proximal [4Fe–4S] cluster of the *A. vinosum* [NiFe] Hase, that in addition is coordinated by one of the carboxylate oxygens of Asp 75 in the small chain of the enzyme, structurally equivalent to the Glu 77 A in *D. vulgaris* Hildenborough (Fig. 8B).

Instead of being released from the cluster as previously believed, the fourth sulfur atom of the cluster becomes attached to one of the oxygens and forms a persulphide bridge with Cys21A. In the Ox1 structure, the oxidation of the proximal [4Fe–4S] cluster is incomplete (*ca.* 80%), with a resulting overlap between the electron densities of both forms of this cluster, hindering the elucidation of the stereochemistry of its oxidized form. In the as-isolated Ox2 crystal structure (1.33 Å resolution), the cluster was found in a *ca.* 100% oxidized form

and confirmed our new interpretation of its chemical structure. The identity of the newly identified sulfur atom was validated by its equivalent isotropic thermal motion parameter (17.2 $Å^2$), very similar to those of Cys21A S^{γ} (17.8 $Å^2$) and O1 (16.1 $Å^2$).

Most stereochemical parameters for the oxidized cluster form were soft-restrained to ensure a well-behaved refinement, using larger σ values (0.05 Å and 5°) than usual to allow for a better accommodation of the atomic positions into the electron density. The stereochemistry of the super-oxidized part of the cluster (near atom Fe2, see Fig. 8A and Supplementary Table 2) was analyzed by comparison with similar parameters retrieved from the Cambridge Structural Database [50,51] and with the exception of the O–S–S motif for which there are few examples, all stereochemical parameters were consistent with the statistical distributions of similar parameters in the CSD (see Supplementary Results for details).

It is very likely that the super-oxidation of the proximal cluster results from O_2 attack during the aerobic purification and/or crystallization of the enzyme. The fact that three oxygen atoms are present in the modified cluster suggests that a water molecule may also be involved. The proximal cluster is surrounded by three conserved water molecules, one of which (W57 in Fig. 8A, W3128 in Fig. 8B and W8 in Fig. 8C) is located between the proximal cluster (*ca.* 4 Å) and the ordered solvent layer (*ca.* 6 Å). A water molecule has also been invoked in oxidation of the active site, as the source of the hydroxo ligand in the Ni-A/Ni-B species, with O_2 acting as the electron acceptor [32,67]. The super-oxidation of the proximal cluster is not observed in the Red1 (not shown) or Red2 (Fig. 8C and Fig. 9) structures of the enzyme, showing that it is reversed upon reduction. Furthermore, the fact that this modification is still not present in the ReOx24 structure (not shown) indicates that this reaction is a slow process that did not occur after 24 h incubation at 20 °C.

This is the first evidence that inactivation of the *D. vulgaris* [NiFeSe] Hase by O_2 involves the super-oxidation of the proximal [4Fe–4S] cluster, which may then act as a barrier against electron transfer with the active site, whereas in [NiFe] Hases the enzyme inactivation mainly results from the binding of an oxygen species at the bridging position of the active site. In addition, it also appears that full oxidation of the proximal cluster is not easily reversed by H_2, since we could not obtain Red2 crystals from Ox2 crystals (where the proximal center is ~100% oxidized to [4Fe–4S–3O]) by using only H_2 in a N_2/H_2 (85/15%) gas mix at ~1 atm, and in the absence of equipment for exposing the crystals to H_2 at high pressure as used by other authors [49], the Red2 crystals could only be obtained after addition of dithionite. This was not the case with the preparation of Red1 crystals from Ox1 crystals, where reduction (as indicated by blue color of methyl viologen) was achieved only with H_2, and thus it seems that a reasonable number of active molecules with intact clusters in the oxidized crystal (as in Ox1) are needed in order to supply electrons by intermolecular transfer to reduce the oxidized clusters of neighboring molecules and restore their canonical composition and stereochemistry. In a crystal where very few if any intact clusters are present (as in Ox2), this process may be extremely slow or even impossible.

The recent crystallographic structures of O_2-tolerant [NiFe] Hases from *Hydrogenovibrio marinus* (PDB 3ayx), *Ralstonia euthropha* (PDB 3rgw) and *E. coli* (PDB 3uqy) showed that the proximal iron–sulfur cluster is of the form [4Fe–3S] and is coordinated by six cysteine residues [19,22,23] (Fig. 8D). In O_2-sensitive [NiFe] Hases and in [NiFeSe] Hases, where the proximal [4Fe–4S] cluster is coordinated by four cysteine residues, the two additional cysteines correspond to conserved glycine residues (Supplementary Fig. 1). One of the sulfur atoms of the [4Fe–3S] cluster, equivalent to S2 in the Ox1 and Ox2 structures (Fig. 8A), and S3 in the Red1, Red2 and ReOx24 structures (Fig. 8C), is replaced by S^{γ} from Cys 19 (3rgw and 3uqy) or Cys 25 (3ayx) in the small sub-units of the O_2-tolerant enzymes. The sixth cysteine residue is structurally equivalent to Gly 126A in *D. vulgaris* [NiFeSe] Hase and coordinates atom Fe3 in the proximal cluster (Fig. 8C). As a result of these two structural changes, one of the Fe–S bonds is broken in the cluster and it assumes a distorted geometry in the O_2-tolerant enzymes. Several studies have pointed to this cluster as responsible for the O_2 tolerance displayed by this type of Hases [12,18,20,21,68], and it has been proposed that it can undergo two redox transitions instead of the single one that can take place in the canonical $[4Fe–4S]^{2+/1+}$ cluster. This property allows reverse donation of two electrons to the active site, thus preventing the O_2-tolerant enzymes from reaching the unready Ni-A state [20]. Instead, their inactive state is always of the ready Ni-B form. It is also worth noting that in the crystal structures of the O_2-tolerant Hases one of the conserved water molecules near the proximal cluster (W57 in Ox2, see Fig. 8A) is no longer present because of the steric hindrance due to the side chain of the sixth cysteine residue (Cys 120S in the O_2-tolerant *E. coli* [NiFe] Hase, PDB 3uqy, see Fig. 8D). This observation raises the intriguing possibility that the role of this sixth cysteine, which has been established not to be relevant to the mechanism of O_2-tolerance involving the two redox states of the proximal [4Fe–3S] cluster [21], may be instead to protect this cluster from O_2 attack in a process similar to that resulting in a [Fe4–S4–O3] proximal cluster as observed in the Ox1 and Ox2 structures of the *D. vulgaris* [NiFeSe] Hase.

4. Conclusions

The crystal structure of the soluble form of the [NiFeSe] Hase from the sulfate-reducing bacterium *D. vulgaris* Hildenborough was determined in three redox forms: as-isolated oxidized (Ox1 and Ox2), reduced (Red1 and Red2) and re-oxidized (ReOx24). Both oxidized crystal structures were determined to higher resolution (1.5 Å and 1.33 Å, respectively) than the previously reported crystal structure of the same form (2.04 Å) [37], thus providing a more detailed structural picture of the oxidized form of this enzyme, which was essential to elucidate the structure of the modified proximal cluster. The 3D structure of the *D. vulgaris* [NiFeSe] Hase is largely identical to that of a classic [NiFe] Hase, but there are important differences around the [NiFe] binuclear active site. In the structures of the as-isolated oxidized forms Ox1 and Ox2, the Se atom in Sec489B is present in three conformations, termed conformers I, II and III, with conformer I being predominant. These

conformers correspond to the three different rotamers of Sec489B (defined by the dihedral angles about the C^{α}–C^{β} bond). The structures of the other two redox states reveal a geometry of the active site where the Sec489B is in similar conformations to conformers II and III. In the Red1 structure only conformer III is detected, while in the Red2 structure a small conformer II component is also observed. Conformer III corresponds to the only conformer observed for the equivalent cysteine residue in [NiFe] Hases and is also observed in the crystal structure of the [NiFeSe] Hase from *Dm. baculatum* in the reduced state [49]. In the crystal structure of the re-oxidized enzyme (ReOx24), conformers II and III of Sec489B are present, with a predomination of conformer III. In conformers I and II an exogenous sulfur atom binds the Se atom of Sec489B (and also the Ni atom in the case of conformer I). It appears that it is the binding of this S atom, rather than the oxidation state, that determines which conformer is present. This binding is apparently a slow process compared to the reduction/re-oxidation of the protein, resulting in a mixture of conformers in different oxidation states. The consequence of the conformational changes of Sec489B in comparison to the corresponding Cys residue in [NiFe] Hases is that the Se atom blocks access to the bridging position of the active site of small molecular species such as O_2, and thus may prevent the formation of a bridging oxo-ligand, usually implicated in the Ni-A and Ni-B electronic states of [NiFe] Hases [13,69]. However, recent experiments have shown that the Ni-A/Ni-B states can also be reached in the absence of O_2, but in the presence of strong oxidizing agents or a high redox potential, which possibly generate reactive oxygen species close to the active site [32]. Also, in contrast with O_2-sensitive and O_2-tolerant [NiFe] Hases, the Ni–Fe distance in the [NiFeSe] Hase increases slightly upon reduction of the as-isolated oxidized form, a larger increase being observed when the reduced form is allowed to reoxidize in air. An additional feature observed at the active site of the *D. vulgaris* [NiFeSe] Hase is the oxidation of the terminal cysteine bound to the Ni atom to cysteine sulfinic acid/sulfinate. This modification is not reversible by reduction of the enzyme under the conditions used.

Finally, the high-resolution structures of the oxidized state enabled the structural and stereochemical elucidation of the modification of the proximal-iron–sulfur cluster that was found oxidized to a [4Fe–4S–3O] form. A similar form of this cluster was previously reported for the three-dimensional structure of the O_2-sensitive [NiFe] Hase from *D. desulfuricans* ATCC 27774 [65], and may result from O_2 attack involving also a water molecule, during aerobic purification and/or crystallization. The higher resolution (1.5 Å and 1.33 Å respectively) of the Ox1 and Ox2 crystal structures allowed the clarification of the chemical composition of the modified cluster, showing that one of the sulfur atoms was not lost as previously believed [37,65], but instead formed a persulfide bridge with a cysteine coordinating the unmodified cluster. Three water molecules around the proximal iron–sulfur cluster are conserved in the known 3D structures of O_2-sensitive [NiFe] Hases, revealing a certain degree of solvent exposure of this cluster, even though it is buried inside the protein, whereas in the known 3D structures of O_2-tolerant [NiFe] Hases one of these three molecules is displaced by one of the extra Cys residues coordinating the proximal iron–sulfur cluster. In the oxidized crystal structure Ox2 the proximal iron–sulfur cluster was almost completely oxidized to [4Fe–4S–3O]. Contrary to our experience with the Ox1 sample where the proximal iron–sulfur cluster was ca. 80% oxidized to [4Fe–4S–3O], crystal reduction of Ox2 with a mixture of H_2/N_2 at 1 atm was not possible. Thus, it is becoming increasingly apparent that oxidation of the proximal iron–sulfur cluster may be an important modification in the inactivation of some O_2-sensitive [NiFe] and [NiFeSe] Hases. In fact, it is still not clear what the difference between the Ni-A and Ni-B inactivated states is, as the hydroperoxo bridging ligand believed to correspond to the Ni-A state of *D. fructosovorans* [NiFe] Hase (PDB 1yqw) [69] is not present in the *A. vinosum* [NiFe] Hase in the same state (PDB 3myr) [17]. The proposal for a hydroperoxo ligand stemmed from the fact that an elongated electron density was observed at the bridging position [69]. The high-resolution (1.04 Å) crystal structure of the [NiFe] Hase from *D. vulgaris* Myiazaki F in the Ni-A state (PDB 1wui) [56] also displayed a diatomic oxygen species at the bridging position of the NiFe active site, along with the partial oxidation to sulfenate of one of the bridging cysteines and of the terminal cysteine coordinating the Ni atom that corresponds to Sec489B in the [NiFeSe] Hase from *D. vulgaris* Hildenborough. However, it is also conceivable that the electron density assigned to a diatomic oxygen species in both Ni-A structures may actually represent two different positions of an hydroxo ligand: one in a bridging position between the Ni and Fe atoms, and a second where the oxo-species only coordinates the Ni atom with a coordination distance of *ca.* 2 Å.

The Ni-A and Ni-B states have very similar spectroscopic properties (namely in FT-IR that is extremely sensitive to the active site electronic state), pointing to similar configurations of the active site. Indeed, our results suggest that the difference between the two states might also involve in some cases the oxidation state of the proximal cluster, as similar modifications seem to be present in the crystal structures of the O_2-sensitive Hases from *A. vinosum* [17] and *D. desulfuricans* ATCC 27774 [65]. Thus, the Ni-A state in O_2-sensitive Hases could arise from different structural features at or near the active site in different enzymes, rather than a single one as usually believed. In addition, it seems that different enzymes may form different oxidized species. In this context, it should be noted that very different protocols can be used to originate Ni-A species, such as the case of the *A. vinosum* [NiFe] Hase that was aerobically purified already mainly in the Ni-A state [17], whereas the Ni-A state of the *D. vulgaris* Myiazaki F [NiFe] Hase was obtained by treatment with Na_2S [56]. The small changes in FTIR frequencies and EPR *g*-values between O_2-sensitive [NiFe] Hases in the Ni-A and Ni-B states may be rationalized in terms of small structural changes closer to the Ni atom or larger structural changes further away. The bridging ligand is typically ca. 2 Å from the Ni atom whereas the center of the proximal Fe–S cluster is *ca.* 13 Å distant from the Ni atom. However, in the case of the *A. vinosum* [NiFe] Hase there is no evident structural change at or near the active site other than the oxidized proximal Fe–S that can account for the Ni-A state of the enzyme in the crystal. Furthermore, a more distant interaction of Ni^{3+} with the medial [3Fe–4S] cluster has been implicated in the complex splitting of EPR *g*-signals from some [NiFe] Hases, possibly mediated by an extra Fe^{3+} species

located close to or in a modified proximal Fe–S cluster (see Ref. [17] and references therein).

The understanding of the structural factors behind the different behavior displayed by [NiFeSe] Hases in comparison with O_2-sensitive [NiFe] Hases has become a subject of our research, since [NiFeSe] Hases can be used in biotechnological applications, as shown by the performance of *Dm. baculatum* [NiFeSe] hydrogenase in experimental H_2-producing devices [10,29] and the direct electron transfer observed after immobilization *of D. vulgaris* [NiFeSe] Hase in gold electrodes [27,30].

The crystals structures reported herein provide important insights into how [NiFeSe] Hases are inactivated by O_2. A main achievement is the elucidation of the structure of the modified proximal FeS cluster upon inactivation, which seems to involve reaction with O_2 and also a water molecule. Our results show that this modification is a slow process that is reversible upon reduction, in contrast to the formation of a cysteine-sulfinic acid at the active site, which is still present in the reduced form of the enzyme. Further detailed time-resolved studies of this enzyme are planned to evaluate the relative timing of these two oxidative processes, and their relative impact on the catalytic activity of the enzyme. These studies will be essential for the future design of engineered proteins with enhanced oxygen tolerance and catalytic properties to be used in bio-hydrogen production or hydrogen-based bioelectrical devices.

Acknowledgments

This work is based on experiments performed at the Swiss Light Source (SLS), Paul Scherrer Institute, Villigen, Switzerland and at the European Synchrotron Radiation Facility (ESRF), Grenoble, France. The research leading to these results has received funding from the European Community's Seventh Framework Programme (FP7/2007–2013) under grant agreement no. 226716, and it was also supported by research grants PTDC/BIA-PRO/70429/2006 and PEst-OE/EQB/LA0004/2011 funded by Fundação para a Ciência e Tecnologia (Portugal). The authors thank the ESRF for support and João Carita for growing the bacterial cells.

Appendix A. Supplementary data

Supplementary data related to this article can be found at http://dx.doi.org/10.1016/j.ijhydene.2013.04.132.

REFERENCES

[1] Lee HS, Vermaas WF, Rittmann BE. Biological hydrogen production: prospects and challenges. Trends Biotechnol 2010;28:262–71.
[2] Friedrich B, Fritsch J, Lenz O. Oxygen-tolerant hydrogenases in hydrogen-based technologies. Curr Opin Biotechnol 2011;22:358–64.
[3] Lojou E. Hydrogenases as catalysts for fuel cells: strategies for efficient immobilization electrode interfaces. Electrochim Acta 2011;56:10385–97.
[4] Vignais PM, Billoud B, Meyer J. Classification and phylogeny of hydrogenases. FEMS Microbiol Rev 2001;25:455–501.
[5] Vignais PM, Billoud B. Occurrence, classification, and biological function of hydrogenases: an overview. Chem Rev 2007;107:4206–72.
[6] Cracknell JA, Wait AF, Lenz O, Friedrich B, Armstrong FA. A kinetic and thermodynamic understanding of O_2 tolerance in [NiFe]-hydrogenases. Proc Natl Acad Sci USA 2009;106:20681–6.
[7] Goldet G, Wait AF, Cracknell JA, Vincent KA, Ludwig M, Lenz O, et al. Hydrogen production under aerobic conditions by membrane-bound hydrogenases from *Ralstonia* species. J Am Chem Soc 2008;130:11106–13.
[8] Vincent KA, Cracknell JA, Lenz O, Zebger I, Friedrich B, Armstrong FA. Electrocatalytic hydrogen oxidation by an enzyme at high carbon monoxide or oxygen levels. Proc Natl Acad Sci USA 2005;102:16951–4.
[9] Burgdorf T, Lenz O, Buhrke T, van der Linden E, Jones AK, Albracht SP, et al. [NiFe]-hydrogenases of *Ralstonia eutropha* H16: modular enzymes for oxygen-tolerant biological hydrogen oxidation. J Mol Microbiol Biotechnol 2005;10:181–96.
[10] Armstrong FA, Belsey NA, Cracknell JA, Goldet G, Parkin A, Reisner E, et al. Dynamic electrochemical investigations of hydrogen oxidation and production by enzymes and implications for future technology. Chem Soc Rev 2009;38:36–51.
[11] Armstrong FA, Wait AF, Parkin A, Morley GM, dos Santos L. Characteristics of enzyme-based hydrogen fuel cells using an oxygen-tolerant hydrogenase as the anodic catalyst. J Phys Chem C 2010;114:12003–9.
[12] Pandelia ME, Nitschke W, Infossi P, Giudici-Orticoni MT, Bill E, Lubitz W. Characterization of a unique [FeS] cluster in the electron transfer chain of the oxygen tolerant [NiFe] hydrogenase from *Aquifex aeolicus*. Proc Natl Acad Sci USA 2011;108:6097–102.
[13] De Lacey AL, Fernandez VM, Rousset M, Cammack R. Activation and inactivation of hydrogenase function and the catalytic cycle: spectroelectrochemical studies. Chem Rev 2007;107:4304–30.
[14] Liebgott P-P, Dementin S, Leger C, Rousset M. Towards engineering O_2-tolerance in [Ni-Fe] hydrogenases. Energ Environ Sci 2011;4:33–41.
[15] van Gastel M, Stein M, Brecht M, Schroder O, Lendzian F, Bittl R, et al. A single-crystal ENDOR and density functional theory study of the oxidized states of the [NiFe] hydrogenase from *Desulfovibrio vulgaris* Miyazaki F. J Biol Inorg Chem 2006;11:41–51.
[16] Fontecilla-Camps JC, Volbeda A, Cavazza C, Nicolet Y. Structure/function relationships of [NiFe]- and [FeFe]-hydrogenases. Chem Rev 2007;107:4273–303.
[17] Ogata H, Kellers P, Lubitz W. The crystal structure of the [NiFe] hydrogenase from the photosynthetic bacterium *Allochromatium vinosum*: characterization of the oxidized enzyme (Ni-A state). J Mol Biol 2010;402:428–44.
[18] Fritsch J, Loscher S, Sanganas O, Siebert E, Zebger I, Stein M, et al. [NiFe] and [FeS] cofactors in the membrane-bound hydrogenase of *Ralstonia eutropha* investigated by X-ray absorption spectroscopy: insights into O_2-tolerant H_2 cleavage. Biochemistry 2011;50:5858–69.
[19] Fritsch J, Scheerer P, Frielingsdorf S, Kroschinsky S, Friedrich B, Lenz O, et al. The crystal structure of an oxygen-tolerant hydrogenase uncovers a novel iron–sulphur centre. Nature 2011;479:249–52.
[20] Goris T, Wait AF, Saggu M, Fritsch J, Heidary N, Stein M, et al. A unique iron–sulfur cluster is crucial for oxygen tolerance of a [NiFe]-hydrogenase. Nat Chem Biol 2011;7:648.
[21] Lukey MJ, Roessler MM, Parkin A, Evans RM, Davies RA, Lenz O, et al. Oxygen-tolerant [NiFe]-hydrogenases: the

individual and collective importance of supernumerary cysteines at the proximal Fe–S cluster. J Am Chem Soc 2011;133:16881–92.
[22] Shomura Y, Yoon K-S, Nishihara H, Higuchi Y. Structural basis for a [4Fe–3S] cluster in the oxygen-tolerant membrane-bound [NiFe]-hydrogenase. Nature 2011;479:253–6.
[23] Volbeda A, Amara P, Darnault C, Mouesca JM, Parkin A, Roessler MM, et al. X-ray crystallographic and computational studies of the O_2-tolerant [NiFe]-hydrogenase 1 from *Escherichia coli*. Proc Natl Acad Sci USA 2012;109:5305–10.
[24] Baltazar CSA, Marques MC, Soares CM, DeLacey AM, Pereira IAC, Matias PM. Nickel–iron–selenium hydrogenases – an overview. Eur J Inorg Chem 2011:948–62.
[25] Valente FMA, Oliveira ASF, Gnadt N, Pacheco I, Coelho AV, Xavier AV, et al. Hydrogenases in *Desulfovibrio vulgaris* Hildenborough: structural and physiologic characterisation of the membrane-bound [NiFeSe] hydrogenase. J Biol Inorg Chem 2005;10:667–82.
[26] Parkin A, Goldet G, Cavazza C, Fontecilla-Camps JC, Armstrong FA. The difference a Se makes? Oxygen-tolerant hydrogen production by the [NiFeSe]-hydrogenase from *Desulfomicrobium baculatum*. J Am Chem Soc 2008;130:13410–6.
[27] Gutierrez-Sanchez C, Rudiger O, Fernandez VM, De Lacey AL, Marques M, Pereira IA. Interaction of the active site of the Ni–Fe–Se hydrogenase from *Desulfovibrio vulgaris* Hildenborough with carbon monoxide and oxygen inhibitors. J Biol Inorg Chem 2010;15:1285–92.
[28] De Lacey AL, Gutierrez-Sanchez C, Fernandez VM, Pacheco I, Pereira IAC. FTIR spectroelectrochemical characterization of the Ni–Fe–Se hydrogenase from *Desulfovibrio vulgaris* Hildenborough. J Biol Inorg Chem 2008;13:1315–20.
[29] Reisner E, Fontecilla-Camps JC, Armstrong FA. Catalytic electrochemistry of a [NiFeSe]-hydrogenase on TiO_2 and demonstration of its suitability for visible-light driven H_2 production. Chem Commun 2009:550–2.
[30] Rüdiger O, Gutiérrez-Sánchez C, Olea D, Pereira IAC, Vélez M, Fernández VM, et al. Enzymatic anodes for hydrogen fuel cells based on covalent attachment of Ni–Fe hydrogenases and direct electron transfer to SAM-modified gold electrodes. Electroanalysis 2010;22:776–83.
[31] Vincent KA, Parkin A, Lenz O, Albracht SP, Fontecilla-Camps JC, Cammack R, et al. Electrochemical definitions of O_2 sensitivity and oxidative inactivation in hydrogenases. J Am Chem Soc 2005;127:18179–89.
[32] Hamdan AA, Burlat B, Gutiérrez-Sanz O, Liebgott P-P, Baffert C, De Lacey AL, et al. O_2-independent formation of the inactive states of NiFe hydrogenase. Nat Chem Biol 2013;9:15–7.
[33] Hamdan AA, Liebgott PP, Fourmond V, Gutierrez-Sanz O, De Lacey AL, Infossi P, et al. Relation between anaerobic inactivation and oxygen tolerance in a large series of NiFe hydrogenase mutants. Proc Natl Acad Sci USA 2012;109:19916–21.
[34] Fritsch J, Lenz O, Friedrich B. Structure, function and biosynthesis of O_2-tolerant hydrogenases. Nat Rev Microbiol 2013;11:106–14.
[35] Valente FAA, Almeida CC, Pacheco I, Carita J, Saraiva LM, Pereira IAC. Selenium is involved in regulation of periplasmic hydrogenase gene expression in *Desulfovibrio vulgaris* Hildenborough. J Bacteriol 2006;188:3228–35.
[36] Valente FMA, Pereira PM, Venceslau SS, Regalla M, Coelho AV, Pereira IAC. The [NiFeSe] hydrogenase from *Desulfovibrio vulgaris* Hildenborough is a bacterial lipoprotein lacking a typical lipoprotein signal peptide. FEBS Lett 2007;581:3341–4.
[37] Marques MC, Coelho R, De Lacey AL, Pereira IAC, Matias PM. The three-dimensional structure of [NiFeSe] hydrogenase from *Desulfovibrio vulgaris* Hildenborough: a hydrogenase without a bridging ligand in the active site in its oxidised, "as-isolated" state. J Mol Biol 2010;396:893–907.
[38] Marques M, Coelho R, Pereira IAC, Matias PM. Purification, crystallization and preliminary crystallographic analysis of the [NiFeSe] hydrogenase from *Desulfovibrio vulgaris* Hildenborough. Acta Crystallogr F 2009;65:920–2.
[39] Kabsch W. Automatic processing of rotation diffraction data from crystals of initially unknown symmetry and cell constants. J Appl Crystallogr 1993;26:795–800.
[40] Winn MD, Ballard CC, Cowtan KD, Dodson EJ, Emsley P, Evans PR, et al. Overview of the CCP4 suite and current developments. Acta Crystallogr D 2011;67:235–42.
[41] Mccoy AJ, Grosse-Kunstleve RW, Adams PD, Winn MD, Storoni LC, Read RJ. Phaser crystallographic software. J Appl Crystallogr 2007;40:658–74.
[42] Potterton E, Briggs P, Turkenburg M, Dodson E. A graphical user interface to the CCP4 program suite. Acta Crystallogr D 2003;59:1131–7.
[43] Adams PD, Afonine PV, Bunkoczi G, Chen VB, Davis IW, Echols N, et al. PHENIX: a comprehensive python-based system for macromolecular structure solution. Acta Crystallogr D 2010;66:213–21.
[44] Emsley P, Lohkamp B, Scott WG, Cowtan K. Features and development of Coot. Acta Crystallogr D 2010;66:486–501.
[45] Painter J, Merritt EA. Optimal description of a protein structure in terms of multiple groups undergoing TLS motion. Acta Crystallogr D 2006;62:439–50.
[46] Chen VB, Arendall III WB, Headd JJ, Keedy DA, Immormino RM, Kapral GJ, et al. MolProbity: all-atom structure validation for macromolecular crystallography. Acta Crystallogr D 2010;66:12–21.
[47] Larkin MA, Blackshields G, Brown NP, Chenna R, McGettigan PA, McWilliam H, et al. Clustal W and Clustal X version 2.0. Bioinformatics 2007;23:2947–8.
[48] Krissinel E, Henrick K. Secondary structure matching (SSM), a new tool for fast protein alignment in three dimensions. Acta Crystallogr D 2004;D60:2256–68.
[49] Garcin E, Vernede X, Hatchikian EC, Volbeda A, Frey M, Fontecilla-Camps JC. The crystal structure of a reduced [NiFeSe] hydrogenase provides an image of the activated catalytic center. Structure 1999;7:557–66.
[50] Allen F. The Cambridge Structural Database: a quarter of a million crystal structures and rising. Acta Crystallogr B 2002;58:380–8.
[51] Bruno IJ, Cole JC, Edgington PR, Kessler M, Macrae CF, McCabe P, et al. New software for searching the Cambridge Structural Database and visualizing crystal structures. Acta Crystallogr B 2002;58:389–97.
[52] Parkin A, Sargent F. The hows and whys of aerobic H_2 metabolism. Curr Opin Chem Biol 2012;16:26–34.
[53] Fujiwara N, Nakano M, Kato S, Yoshihara D, Ookawara T, Eguchi H, et al. Oxidative modification to cysteine sulfonic acid of Cys111 in human copper–zinc superoxide dismutase. J Biol Chem 2007;282:35933–44.
[54] Jacob C, Holme AL, Fry FH. The sulfinic acid switch in proteins. Org Biomol Chem 2004;2:1953–6.
[55] Romão MJ, Coelho C, Gonzalez PJ, Moura JJG, Moura I, Trincão J. The crystal structure of *Cupriavidus necator* nitrate reductase in oxidized and partially reduced states. J Mol Biol 2011;408:932–48.
[56] Ogata H, Hirota S, Nakahara A, Komori H, Shibata N, Kato T, et al. Activation process of [NiFe] hydrogenase elucidated by high-resolution X-ray analyses: conversion of the ready to the unready state. Structure 2005;13:1635–42.

[57] Reddie KG, Carroll KS. Expanding the functional diversity of proteins through cysteine oxidation. Curr Opin Chem Biol 2008;12:746–54.
[58] Leonard SE, Carroll KS. Chemical 'omics' approaches for understanding protein cysteine oxidation in biology. Curr Opin Chem Biol 2011;15:88–102.
[59] Pandelia ME, Ogata H, Lubitz W. Intermediates in the catalytic cycle of [NiFe] hydrogenase: functional spectroscopy of the active site. ChemPhysChem 2010;11:1127–40.
[60] Wilson MA. The role of cysteine oxidation in DJ-1 function and dysfunction. Antioxid Redox Signal 2011;15:111–22.
[61] Buonomo RM, Font I, Maguire MJ, Reibenspies JH, Tuntulani T, Darensbourg MY. Study of sulfinate and sulfenate complexes derived from the oxygenation of thiolate sulfur in [1,5-bis(2-mercapto-2-methylpropyl)-1,5-diazacyclooctanato(2-)]nickel(II). J Am Chem Soc 1995;117:963–73.
[62] Matthew Cocker T, Bachman RE. Isolation and crystal structure of a novel dinuclear nickel(II) O-bound sulfinate from the oxidation of 2,2′-bipyridine-1,2-benzenedithiolatonickel(II). Chem Commun 1999:875–6.
[63] Robertson N, Parsons S, Awaga K, Fujita W. Structural characteristics of dithiolene and nitronyl nitroxide salts: a unique oxygenation/deoxygenation process. CrystEngComm 2000;2:121–4.
[64] Bolligarla R, Das SK. Sulfur oxygenation of [Ni(btdt)2]2^- by aerial oxidation under ambient conditions – syntheses, crystal structures, and properties of $[Bu_4N]_2[Ni(btdt)_2]$ and $[Bu_4N]_2[Ni(btdtO_2)_2]\cdot H_2O$ ({btdt}$2^- = 2,1,3$-benzenethiadiazole-5,6-dithiolate). Eur J Inorg Chem 2012;2012:2933–9.
[65] Matias PM, Soares CM, Saraiva LM, Coelho R, Morais J, Le Gall J, et al. [NiFe] hydrogenase from *Desulfovibrio desulfuricans* ATCC 27774: gene sequencing, three-dimensional structure determination and refinement at 1.8 Å and modelling studies of its interaction with the tetrahaem cytochrome c_3. J Biol Inorg Chem 2001;6:63–81.
[66] Aragão D, Mitchell EP, Frazao CF, Carrondo MA, Lindley PF. Structural and functional relationships in the hybrid cluster protein family: structure of the anaerobically purified hybrid cluster protein from *Desulfovibrio vulgaris* at 1.35 Å resolution. Acta Crystallogr D 2008;64:665–74.
[67] Carepo M, Tierney DL, Brondino CD, Yang TC, Pamplona A, Telser J, et al. 17O ENDOR detection of a solvent-derived Ni–(OH_x)–Fe bridge that is lost upon activation of the hydrogenase from *Desulfovibrio gigas*. J Am Chem Soc 2002;124:281–6.
[68] Saggu M, Ludwig M, Friedrich B, Hildebrandt P, Bittl R, Lendzian F, et al. Impact of amino acid substitutions near the catalytic site on the spectral properties of an O_2-tolerant membrane-bound [NiFe] hydrogenase. ChemPhysChem 2010;11:1215–24.
[69] Volbeda A, Martin L, Cavazza C, Matho M, Faber BW, Roseboom W, et al. Structural differences between the ready and unready oxidized states of [NiFe] hydrogenases. J Biol Inorg Chem 2005;10:239–49.
[70] Diederichs K, Karplus PA. Improved R-factors for diffraction data analysis in macromolecular crystallography. Nat Struct Biol 1997;4:269–75.
[71] Matthews BW. Solvent content of protein crystals. J Mol Biol 1968;33:491–7.
[72] Cruickshank DW. Remarks about protein structure precision. Acta Crystallogr D 1999;55:583–601.